

**NUMERICAL INVESTIGATION OF MIXED CONVECTION HEAT
TRANSFER IN PRESENCE OF MAGNETIC FIELD IN A LID-
DRIVEN WAVY CAVITY HAVING VERTICAL FIN**

Thesis submitted for the award of the degree of
Master of Science
at the Bangladesh University of Engineering and Technology

by

Md. Fayz-Al-Asad

Student No. 1017092501F

Registration No. 1017092501, Session: October- 2017



Department of Mathematics
Bangladesh University of Engineering and Technology (BUET),
Dhaka-1000, Bangladesh

July - 2019


The Thesis Titled
**Numerical Investigation of Mixed Convection Heat Transfer in Presence of
Magnetic Field in a Lid-driven Wavy Cavity Having Vertical Fin**


Submitted by
Md. Fayz-Al-Asad


Student No: 1017092501F, Registration No: 1017092501, Session: October 2017,
a full-time student of M. Sc. (Mathematics) has been accepted as satisfactory in
partial fulfillment of the requirement for the award of the degree of

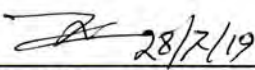
Master of Science in Mathematics
on July 28, 2019

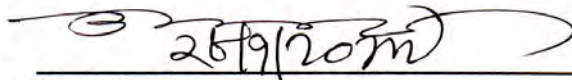
BOARD OF EXAMINERS

1. 

Dr. Md. Manirul Alam Sarker Chairman
Professor (Supervisor)
Department of Mathematics, BUET, Dhaka-1000
2. 

Dr. Md. Mustafizur Rahman Member
Professor and Head (Ex-Officio)
Department of Mathematics, BUET, Dhaka-1000
3. 

Dr. Md. Abdul Maleque Member
Professor
Department of Mathematics, BUET, Dhaka-1000
4. 

Dr. Md. Zafar Iqbal Khan Member
Professor
Department of Mathematics, BUET, Dhaka-1000
5. 

Dr. Md. Tajul Islam Member
Professor (External)
Department of Mathematics,
Begaum Rokeya University, Rangpur

AUTHOR'S DECLARATION

I hereby announce that the work which is being presented in this dissertation entitled **“Numerical Investigation of Mixed Convection Heat Transfer in Presence of Magnetic Field in a Lid-driven Wavy Cavity Having Vertical Fin”** submitted in partial fulfillment of the requirements for the award of the degree of **Master of Science** in Mathematics in the Department of Mathematics, Bangladesh University of Engineering and Technology (BUET), Dhaka is an authentic record of my own work.

It is hereby declared that this thesis or any part of it has not been submitted elsewhere (University or Institution) for the award of any degree or diploma.

Fayz-Al-Asad

Md. Fayz-Al-Asad

M. Sc. Student

Department of Mathematics

July 28, 2019

This work is dedicated
To
My beloved Parents

ACKNOWLEDGEMENT

First and foremost, I would like to express my special gratitude towards ‘ALLAH’ who has given me the capability to come in this position and to complete the thesis work successfully.

I am especially indebted to my supervisor Professor **Dr. Md. Manirul Alam Sarker**, Department of Mathematics, Bangladesh University of Engineering and Technology (BUET), Dhaka, for his scholastic supervision, erudite discussion, invaluable suggestion, continuous encouragement and mental support throughout the progress of this work.

I am indebted to Professor Dr. Md. Mustafizur Rahman, Head, Department of Mathematics, Bangladesh University of Engineering and Technology (BUET), Dhaka, for his encouragement and hearty cooperation.

I am grateful to Professor Dr. Md. Abdul Maleque, and Professor Dr. Md. Zafar Iqbal Khan, Department of Mathematics, Bangladesh University of Engineering and Technology (BUET), Dhaka, for their heartiest level of cooperation, valuable advice friendly discussions and encouragement at the different stages of my research work.

I would like to thank all the respected teachers of this department for their cooperation and valuable advices.

I would also like to thank my friends for their diligent assistance throughout the period of this thesis. Finally, words alone cannot express my thanks I owe to my lovely parents and siblings for their wise counsel and sympathetic ear.

Md. Fayz-Al-Asad

July 28, 2019

ABSTRACT

Mixed convection heat transfer in presence of magnetic field in a lid-driven wavy cavity having vertical fin has been studied numerically in this thesis. The horizontal bottom and top walls are kept at constant heated temperature T_h while the vertical wavy walls are kept at constant cold temperature T_c maintaining $T_h > T_c$. A heated fin of length (l) is attached to the hot bottom wall at a position (d) from the left wall having thickness (b). The top wall moves right to left with constant velocity. The gravitational force acts in vertically downward direction and a uniform magnetic field with a constant magnitude in the direction of the moving lid is applied. The physical problems are presented mathematically by different sets of governing equations along with the corresponding boundary conditions. Using a set of appropriate transformations, the governing equations along with the boundary conditions are transformed into non-dimensional form, which is then solved by employing a Finite-element method based on Galerkin weighted residuals.

The investigations are conducted for different values of Richardson number (Ri), Hartmann number (Ha), fin lengths (L) but for fixed fin thickness, fin position, amplitude, number of oscillations with $Re = 100$ whereas Prandtl number is kept constant at 0.71. Various characteristics such as streamlines, isotherms, velocity profiles, local Nusselt number, fin effectiveness (ϵ_f) and heat transfer rate in terms of the average Nusselt number (Nu_{av}) and average fluid temperature (θ_{av}) are presented for the aforementioned parameters.

The results indicate that the mentioned parameters strongly affect the flow phenomenon and temperature field inside the wavy cavity whereas on the fin length these effects are more significant. Results of this study conformed very well with the published ones.

TABLE OF CONTENTS

<u>Items</u>	<u>Page</u>
BOARD OF EXAMINERS	Error! Bookmark not defined.
AUTHOR'S DECLARATION	ii
ACKNOWLEDGEMENT	v
ABSTRACT	vi
NOMENCLATURE	x
LIST OF TABLES	xii
LIST OF FIGURES	xiii
CHAPTER 1	1
INTRODUCTION	1
1.1 MODES OF HEAT TRANSFER	2
1.2 RELEVANT DEFINITIONS	3
1.2.1 Viscosity	3
1.2.2 Viscous Flow	3
1.2.3 Newton's Law of Viscosity	4
1.2.4 Newtonian Fluid	4
1.2.5 Compressibility	4
1.2.6 Incompressible Flow	4
1.2.7 Thermal Diffusivity	4
1.2.8 Thermal Conductivity	5
1.2.9 Magnetohydrodynamics	5
1.2.10 Fin Effectiveness	6
1.3 DIMENSIONLESS PARAMETERS	7
1.3.1 Prandtl Number	7
1.3.2 Richardson Number	7
1.3.3 Reynolds Number.....	8
1.3.4 Hartmann Number.....	9
1.4 MIXED CONVECTION HEAT TRANSFER IN CAVITIES	9
1.5 LITERATURE REVIEW	10
1.6 PARTICULAR APPLICATIONS	14
1.7 OBJECTIVES OF THE PRESENT STUDY	15
1.7.1 Objectives with Specific Aims	15
1.7.2 Possible Outcome	15
1.8 OUTLINE OF THE THESIS	16

CHAPTER 2	17
COMPUTATIONAL TECHNIQUE.....	17
2.1 MERITS AND DEMERITS OF NUMERICAL METHOD.....	18
2.2 ELEMENTS OF NUMERICAL SOLUTION METHODS.....	20
2.2.1 Mathematical Model	20
2.2.2 Discretization Process	20
2.2.3 Numerical Grid.....	21
2.2.4 Finite Approximations	21
2.2.5 Solution Technique	21
2.3 DISCRETIZATION APPROACHES.....	21
2.4 FINITE ELEMENT METHOD	22
2.4.1 Mesh Generation	23
2.4.2 Computational Technique	24
2.5 ALGORITHM.....	24
2.5.1 Solution of System of Equations.....	25
CHAPTER 3	27
MATHEMATICAL MODELLING.....	27
3.1 PHYSICAL CONFIGURATIONS	27
3.2 GOVERNING EQUATIONS ALONG WITH BOUNDARY CONDITIONS..	28
3.2.1 Dimensional Boundary Conditions	29
3.2.2 Dimensional Analysis	29
3.2.3 Boundary Conditions (non-dimensional).....	30
3.2.4 Nusselt Number.....	30
3.3 NUMERICAL ANALYSIS	31
3.3.1 Finite Element Formulation and Computational Procedure.....	31
3.3.2 Grid Size Sensitivity Test.....	36
3.3.3 Validation of the Numerical Scheme	37
CHAPTER 4	39
RESULTS AND DISCUSSION	39
4.1 CASE 1 (Effect of Fin Length When $L = 0.25$)	39
4.1.1 Effect of Richardson number	39
4.1.2 Effects of Hartmann number	42
4.1.3 Heat Transfer Rates.....	45
4.2 CASE 2 (Effect of Fin Length When $L = 0.35$)	48
4.2.1 Effect of Richardson number	48
4.2.2 Effects of Hartmann number	51
4.2.3 Heat Transfer Rates.....	54

4.3 CASE 3 (Effect of Fin Length When $L = 0.45$)	56
4.3.1 Effect of Richardson number	57
4.3.2 Effect of Hartmann number	59
4.3.3 Heat Transfer Rates	62
4.4 FIN EFFECTIVENESS.....	65
CHAPTER 5	70
CONCLUSION AND RECOMMENDATIONS.....	70
SUMMARY OF THE MAJOR OUTCOMES.....	70
EXTENSION OF THIS WORK	71
REFERENCES.....	72

NOMENCLATURE

<i>A</i>	amplitude
<i>b</i>	fin thickness
<i>B</i>	dimensionless fin thickness (b/W)
B_0	magnetic induction (Wb/m^2)
C_p	specific heat at constant pressure ($J/kg.K$)
<i>d</i>	fin position
<i>D</i>	dimensionless fin position (d/W)
<i>g</i>	gravitational acceleration (ms^{-2})
h^*	convective heat transfer coefficient ($W/m^2.K$)
<i>Ha</i>	Hartmann number
<i>k</i>	thermal conductivity of fluid ($Wm^{-1}K^{-1}$)
<i>l</i>	fin length
<i>L</i>	dimensionless fin length (l/W)
<i>n</i>	dimensional distance either along x or y direction (m)
<i>N</i>	dimensionless distance either along X or Y direction
Nu_{av}	average Nusselt number
Nu_L	local Nusselt number
<i>p</i>	pressure
<i>P</i>	dimensionless pressure ($pW^2/\rho\alpha^2$)
<i>Pr</i>	Prandtl number
<i>Re</i>	Reynolds number
<i>Ri</i>	Richardson number
<i>T</i>	dimensional fluid temperature (K)
ΔT	dimensional temperature difference (K)
<i>u</i>	velocity in x-direction (m/s)
<i>U</i>	dimensionless horizontal velocity
<i>v</i>	velocity in y-direction (m/s)
<i>V</i>	dimensionless vertical velocity
<i>W</i>	enclosure width and height
<i>x, y</i>	Cartesian coordinates (m)
<i>X, Y</i>	dimensionless Cartesian coordinates

Greek symbols

α	thermal diffusivity (m^2s^{-1})
β	coefficient of thermal expansion (K^{-1})
λ	number of oscillations
θ	dimensionless fluid temperature
ε_f	fin effectiveness
μ	dynamic viscosity of the fluid (m^2s^{-1})
ν	kinematic viscosity of the fluid (m^2s^{-1})
ρ	density of the fluid (kgm^{-3})
σ	fluid electrical conductivity ($\Omega^{-1}\cdot\text{m}^{-1}$)

Subscripts

av	average
f	fin
c	cold
h	hot

LIST OF TABLES

3.1	Grid sensitivity check at $Pr = 0.71$, $Ri = 1$, $\lambda=2$, $L = 0.45$ and $D = 0.50$	37
3.2	Comparison of average Nusselt number on cold wall for $L = 0.20$, $Pr = 0.71$ and $Ra = 10^6$	38
4.1	Numerical values of average Nusselt number against Ha on the right cold wall for selected value Ri while $Pr = 0.71$, $L = 0.25$, $B = 0.04$ and $D = 0.50$	45
4.2	Numerical values of average fluid temperature against Ri for selected value Ha while $Pr = 0.71$, $L = 0.25$, $B = 0.04$ and $D = 0.50$	47
4.3	Numerical values of average Nusselt number against Ha on the right cold wall for selected value Ri while $Pr = 0.71$, $L = 0.35$, $B = 0.04$ and $D = 0.50$	54
4.4	Numerical values of average fluid temperature against Ri for selected value Ha while $Pr = 0.71$, $L = 0.35$, $B = 0.04$ and $D = 0.50$	56
4.5	Numerical values of average temperature of the fluid against Ri for selected value Ha while $Pr = 0.71$, $L = 0.45$, $B = 0.04$ and $D = 0.50$	63
4.6	Numerical values of average temperature of the fluid against Ri for selected value Ha while $Pr = 0.71$, $L = 0.45$, $B = 0.04$ and $D = 0.50$	64
4.7	Numerical values of fin effectiveness as a function of Ri for different values of Ha while $Pr = 0.71$, $L = 0.25$, $B = 0.04$ and $D = 0.50$	65
4.8	Numerical values of fin effectiveness as a function of Ri for different values of Ha while $Pr = 0.71$, $L = 0.35$, $B = 0.04$ and $D = 0.50$	66
4.9	Numerical values of fin effectiveness as a function of Ri for different values of Ha while $Pr = 0.71$, $L = 0.45$, $B = 0.04$ and $D = 0.50$	67
4.10	Numerical values of fin effectiveness as a function of fin length for different values of Ri while $Pr = 0.71$, $Ha = 20$, $B = 0.04$ and $D = 0.50$	68

LIST OF FIGURES

2.1	Current mesh structure of elements for wavy cavity with fin length $L = 0.45$, fin position $D = 0.50$, fin thickness $B = 0.04$, $A = 0.1$ and $\lambda = 2$.	23
2.2	Flow chart of the computational procedure	24
3.1	Schematic diagram of the wavy cavity and boundary conditions	28
3.2	Grid independency study for different elements while $Pr = 0.71$, $Ri = 1$, $Ha = 10$, $A = 0.1$, $\lambda=2$, $L = 0.45$ and $D = 0.50$	37
3.3	Comparison of Streamlines and isotherms with $Pr = 0.71$, $Ra = 10^5$, $B = 0.1$, $L = 0.50$ and $D = 0.75$	38
4.1	Effect of Richardson number on (a) streamlines and (b) isotherms for $L = 0.25$, $Pr = 0.71$, $Ha = 10$ and $\lambda = 2$	40
4.2	Variation of velocity profiles along the horizontal centre line of cavity for $L = 0.25$, $B = 0.04$, $D = 0.50$, $Ha = 10$ and $Pr = 0.71$ varying Ri	41
4.3	Variation of local Nusselt number along the bottom heated wall of cavity for $L = 0.25$, $B = 0.04$, $D = 0.50$, $Ha = 10$ and $Pr = 0.71$ varying Ri	42
4.4	Effect of Hartmann number on (a) streamlines and (b) isotherms for $L = 0.25$, $Pr = 0.71$, $Ri = 1$ and $\lambda = 2$	43
4.5	Variation of velocity profiles along the horizontal centre line of cavity for $L = 0.25$, $B = 0.04$, $D = 0.50$, $Ri = 1$ and $Pr = 0.71$ varying Ha	44
4.6	Variation of local Nusselt number along horizontal centre line of cavity for $L = 0.25$, $B = 0.04$, $D = 0.50$, $Ri = 1$ and $Pr = 0.71$ varying Ha	45
4.7	Variation of the average Nusselt number against Ha for selected value Ri while $Pr = 0.71$, $L = 0.25$, $B = 0.04$ and $D = 0.50$	46
4.8	Variation of the average fluid temperature against Ri for selected value Ha while $Pr = 0.71$, $L = 0.25$, $B = 0.04$ and $D = 0.50$	47
4.9	Effect of Richardson number on (a) streamlines and (b) isotherms for $L = 0.35$, $Pr = 0.71$, $Ha = 10$ and $\lambda = 2$	49

4.10	Variation of velocity profiles along the horizontal centre line of cavity with Richardson number for $L = 0.35$, at $Pr = 0.71$, $Ha = 10$ and $\lambda = 2$	50
4.11	Variation of local Nusselt number along the bottom heated wall of cavity with Richardson number for $L = 0.35$ at $Pr = 0.71$, $Ha = 10$ and $\lambda = 2$	50
4.12	Effect of Hartmann number on (a) streamlines and (b) isotherms for $L = 0.35$, $Pr = 0.71$, $Ri = 1$ and $\lambda = 2$	52
4.13	Variation of velocity profiles along the horizontal centre line of cavity for $L = 0.35$, $B = 0.04$, $D = 0.50$, $Ri = 1$ and $Pr = 0.71$ varying Ha	53
4.14	Variation of local Nusselt number along horizontal centre line of cavity for $L = 0.35$, $B = 0.04$, $D = 0.50$, $Ri = 1$ and $Pr = 0.71$ varying Ha	53
4.15	Variation of the average Nusselt number against Ha for selected value Ri while $Pr = 0.71$, $L = 0.35$, $B = 0.04$ and $D = 0.50$	55
4.16	Variation of the average fluid temperature against Ri for selected value Ha while $Pr = 0.71$, $L = 0.35$, $B = 0.04$ and $D = 0.50$	56
4.17	Effect of Richardson number on (a) streamlines and (b) isotherms for $L = 0.45$, $Pr = 0.71$, $Ha = 10$ and $\lambda = 2$	57
4.18	Variation of velocity profiles along the horizontal centre line of cavity with Richardson number for $L = 0.45$, at $Pr = 0.71$, $Ha = 10$ and $\lambda = 2$	58
4.19	Variation of local Nusselt number along the bottom heated wall of cavity with Richardson number for $L = 0.45$ at $Pr = 0.71$, $Ha = 10$ and $\lambda = 2$	59
4.20	Effect of Hartmann number on (a) streamlines and (b) isotherms for $L = 0.45$, $Pr = 0.71$, $Ri = 1$ and $\lambda = 2$	60
4.21	Variation of velocity profiles along the horizontal centre line of cavity for $L = 0.45$, $B = 0.04$, $D = 0.50$, $Ri = 1$ and $Pr = 0.71$ varying Ha	61
4.22	Variation of local Nusselt number along horizontal centre line of cavity for $L = 0.45$, $B = 0.04$, $D = 0.50$, $Ri = 1$ and $Pr = 0.71$ varying Ha	62
4.23	Variation of the average Nusselt number against Ha for selected value Ri while $Pr = 0.71$, $L = 0.45$, $B = 0.04$ and $D = 0.50$	63

4.24	Variation of the average fluid temperature against Ri for selected value Ha while $Pr = 0.71$, $L = 0.45$, $B = 0.04$ and $D = 0.50$	64
4.25	Variation of fin effectiveness against Ha for selected value of Ri while $Pr = 0.71$, $L = 0.25$, $B = 0.04$ and $D = 0.5$	66
4.26	Variation of fin effectiveness against Ha for for selected value of Ri while $Pr = 0.71$, $L = 0.35$, $B = 0.04$ and $D = 0.5$	67
4.27	Variation of fin effectiveness against Ha for for selected value of Ri while $Pr = 0.71$, $L = 0.45$, $B = 0.04$ and $D = 0.5$	68
4.28	Variation of fin effectiveness against Ri for selected value of L while $Pr = 0.71$, $Ha = 20$, $B = 0.04$ and $D = 0.5$	69

CHAPTER 1

INTRODUCTION

Mixed convection or combined forced convection and free convection, occurs when free convection and forced convection mechanisms act together to transfer heat. This is also defined as situations where both pressure forces and buoyant forces interact. How much each form of convection contributes to the heat transfer is largely determined by the flow, temperature, geometry, and orientation.

The phenomenon of heat transfer was known to a human being even in the primitive age when they used solar energy as a source of heat. Heat transfer in its initial stage was conceived with the invention of fire in the early age of human civilization. Since then its knowledge and use have been progressively increasing each day as it is directly related to the growth of human civilization. With the invention of the steam engine by James Watt in 1765 A. D., the phenomenon of heat transfer got its first industrial recognition and after that its use extended to a great extent and spread out in different spheres of engineering fields. In the past three decades, digital computers, numerical techniques and improvement of numerical models of heat transfer have made it possible to calculate heat transfer of considerable size and thereby create a new approach to the design of heat transfer equipment. More details are available in Hagen [1].

The study of the universe has led to the realization that all physical phenomena are subject to natural laws. The term natural might well be used to describe the framework or system of fundamental and universal importance within this system is the mechanisms for the transfer of heat. Heat transfer is a branch of applied thermodynamics. It estimates the rate at which heat is transferred across the system boundaries subjected to specific temperature differences of the system during the process. Whereas classical thermodynamics deals with the amount of heat transferred during the process. Heat transfer processes have always been an integral part of our environment. To describe the heat transport phenomenon, a strong background of the hydrodynamics, the convective heat transfer mechanism, and the electromagnetic field are prerequisite as they have a symbiotic relationship.

The rest of this introductory chapter is as follows. Since the problem that we shall study in this thesis is MHD mixed convection heat transfer in presence of magnetic field in a lid-driven wavy cavity having vertical fin, we begin with a brief description on modes of heat transfer in section 1.1. Then reviews on relevant definitions and some effective parameters have been given in sections 1.2 and 1.3 respectively. In section 1.4 mixed convection heat transfer in the cavity is discussed shortly. Literature related to this study has been presented briefly in section 1.5. Then the application and objective of the current study are described in sections 1.6 and 1.7. Finally, in section 1.8, a brief outline of the remainder of the thesis has been presented.

1.1 MODES OF HEAT TRANSFER

Heat transfer is the process of transportation of thermal energy from one region to another region as a result of temperature difference. The heat transfer always takes place from higher temperature medium to lower temperature one and heat transfer stops when the two mediums reach the same temperature. More details are available in Hagen [1]. The heat transfer takes places by the distinct mechanisms or modes are:

- Conduction
- Convection and
- Radiation

Conduction is the transfer of energy from the higher energetic particle of a substance to adjacent lower energetic ones as a result of interactions between the particles. Conduction can take place in solids, liquids, or gases. In gases and liquids, conduction is due to the collisions and diffusion of the molecules during their random motion in solids it is due to the combination of vibrations of the molecules in a lattice and the energy transport by free electrons. The rate of heat conduction through a medium depends on the geometry of the medium, its thickness and the material of the medium, as well as the temperature difference across the medium.

Convection is the mechanism of heat transfer through a fluid in the presence of bulk fluid motion resulting from the temperature difference. The convection of heat transfer is of two types: natural convection and forced convection. If the fluid flow

via convection occurs naturally, the convection is called natural (or free) convection. In this case, the fluid motion is set up by buoyancy effects resulting from the density variation caused by the temperature difference in the fluid and gravitational force. On the other hand, if the fluid motion is artificially created by means of external source like a blower or fan, the heat transfer mode is called forced convection.

Radiation is the energy emitted by matter in the form of electromagnetic waves (or photons) as a result of the changes in the electronic configuration of the atom or molecules. Unlike conduction and convection, the transfer of heat by radiation does not require the presence of an intervening medium. In fact, heat transfer by radiation is faster and suffers no reduction in a vacuum. This is how the energy of the sun reaches the earth. Radiation is a volumetric phenomenon, and all solids, liquids, and gases emit, absorb, or transmit radiation to varying degrees. However, radiation is usually considered to be a surface phenomenon for solids that are opaque to thermal radiation such as metals, wood and rocks

1.2 RELEVANT DEFINITIONS

1.2.1 Viscosity

The viscosity of a fluid which is a strong function of temperature is a measure of its resistance to deformation. A friction force develops between two adjacent fluid layers while they move relative to each other and the slower layer tries to slow down the faster layer. This type of internal resistance to flow is quantified by the fluid property viscosity. All fluid flows involve viscous effects to some degree and therefore no fluid is of zero viscosity. As temperature increases, the viscosity of liquids decreases whereas the viscosity of gases increases with temperature by Çengel and Cimbala [2].

1.2.2 Viscous Flow

Such flows are called viscous whose flow patterns are dominated by the viscous properties of the fluid. This arises in fluids where the velocity gradients are comparatively large. The flow close to the walls of the pipes can be treated as viscous flows by Çengel and Cimbala [2].

1.2.3 Newton's Law of Viscosity

If the shearing stress, τ , increases by increasing the force P , the rate of shearing strain also increases in direct proportion to that; $\tau \propto \frac{du}{dy}$ i.e., $\tau = \mu \frac{du}{dy}$, where μ is the dynamic viscosity of the fluid. This principle is known as Newton's law of viscosity by Çengel and Cimbala [2].

1.2.4 Newtonian Fluid

Newtonian fluids are those fluids for which the constant of proportionality i.e. the coefficient of viscosity (μ) does not change with the rate of deformation. In other words, fluids that follow Newton's law of viscosity are known as Newtonian fluids. Water, air and mercury are some examples of Newtonian fluids by Çengel and Cimbala [2].

1.2.5 Compressibility

Compressibility is a property of a fluid that measures the change in density and consequently, the change in the volume of fluid during motion under the action of external forces by Çengel and Cimbala [2]. The compressibility is expressed in terms of Mach number (M) which is defined by $M = \frac{\text{speed of fluid}}{\text{speed of sound}} = \frac{u}{\alpha_0}$

1.2.6 Incompressible Flow

A flow is said to be incompressible if the density remains nearly constant throughout. Therefore, for incompressible flow, the volume of every portion of fluid remains unchanged over the course of its motion. The density of liquids is basically constant and accordingly the flow of liquids is naturally referred to as incompressible by Çengel and Cimbala [2].

1.2.7 Thermal Diffusivity

Thermal diffusivity represents how fast heat diffuses through a material and is defined as $\alpha = \frac{\text{Heat conducted}}{\text{Heat stored}} = \frac{k}{\rho c_p}$

Here the thermal conductivity k represents how well a material conducts heat and the heat capacity ρC_p represents how much energy a material stores per unit volume. Therefore, the thermal diffusivity of material can be viewed as the ratio of the heat conducted through the material to the heat stored per unit volume. A material that has a high thermal conductivity or a low heat capacity will obviously have a large thermal diffusivity. The large thermal diffusivity means that the propagation of heat into the medium is faster. A small value of thermal diffusivity means the heat is mostly absorbed by the material and a small amount of heat is conducted further by Çengel and Cimbala [2].

1.2.8 Thermal Conductivity

Thermal conductivity is defined as the quantity of heat (Q) transmitted through a unit thickness (L) in a direction normal to a surface of unit area (A) due to a unit temperature gradient (ΔT) under steady state conditions and when the heat transfer is dependent only on the temperature gradient by Çengel and Cimbala [2]. In equation form this becomes the following:

$$\text{Thermal Conductivity} = \text{heat} \times \text{distance} / (\text{area} \times \text{temperature gradient})$$

$$\lambda = Q \times L / (A \times \Delta T)$$

1.2.9 Magnetohydrodynamics

Magnetohydrodynamics (MHD) is that branch of science, which deals with the flow of electrically conducting fluids in electric and magnetic fields. The motion of the conducting fluid across the magnetic field generates electric currents which change the magnetic field and the action of the magnetic field on these currents give rise to mechanical forces, which modify the fluid. However, MHD is usually regarded as a very contemporary subject. Probably the largest advance towards an understanding of such phenomena comes from the fields of astrophysics and geophysics. It has long been assumed that most of the matter in the universe is in the plasma or highly ionized state and much of the basic knowledge in the area of electromagnetic fluid dynamics evolved from these studies. Moreover, MHD explains certain natural phenomena. The motions of the sea induce a magnetic field that perturbs the earth's

magnetic field. Alternatively, the electromagnetic force due to the interaction of currents and the earth's magnetic field propels ocean movements. The MHD was originally applied to astrophysical and geophysical problems, where it is still very important. Engineers employ MHD principles in the design of heat exchanger, pumps and flow meters, in space vehicle propulsion, control and re-entry in creating novel power generating systems and developing confinement schemes for controlled fusion. Other potential applications for MHD include electromagnets with fluid conductors, various energy conversion or storage devices, and magnetically controlled lubrication by conducting fluids etc. A detailed discussion of the Magnetohydrodynamics (MHD) can be found in Shercliff [3].

1.2.10 Fin Effectiveness

Fin effectiveness is the parameter that quantifies the heat transfer enhancement inside the cavity with a fin compared to the case with no fin and is defined as follows

$$\varepsilon_f = \frac{\text{heat transfer with fin}}{\text{heat transfer without fin}}$$

$$\therefore \varepsilon_f = \frac{Q_{\text{fin}}}{Q_{\text{without fin}}}$$

Effectiveness of $\varepsilon_f = 1$ indicates that the addition of fins to the surface does not affect heat transfer at all. That is, heat conducted to the fin through the base area A_b is equal to the heat transferred from the same area A_b to the surrounding medium

Effectiveness of $\varepsilon_f < 1$ indicates that the fin actually acts as insulation, slowing down the heat transfer from the surface. This situation can occur when fins made of low thermal conductivity materials are used.

Effectiveness of $\varepsilon_f > 1$ indicates that the fins are enhancing heat transfer from the surface, as they should. However, the use of fins cannot be justified unless ε_f is sufficiently larger than 1. Finned surfaces are designed on the basis of maximizing the effectiveness of a specified cost or minimizing cost for the desired effectiveness. More details are available in Hagen [1].

1.3 DIMENSIONLESS PARAMETERS

The dimensionless parameters can be considered as measures of the relative importance of certain aspects of the flow. Some dimensionless parameters related to the present study are discussed below:

1.3.1 Prandtl Number

The relative thickness of the velocity and the thermal boundary layers are best described by the dimensionless parameter Prandtl number, defined as

$$Pr = \frac{\nu}{\alpha} = \frac{\text{Viscous diffusion rate}}{\text{Thermal diffusion rate}} = \frac{c_p \mu}{k}$$

Where ν is the kinematic viscosity, $\nu = \frac{\mu}{\rho}$, α is the thermal diffusivity and

$\alpha = \frac{k}{(\rho c_p)}$, μ is the dynamic viscosity, k is the thermal conductivity, c_p is the

specific heat and ρ is the density. It is named after Ludwig Prandtl, who introduced the concept of the boundary layer in 1904 and made significant contributions to boundary layer theory. The Prandtl number of fluids ranges from less than 0.01 for liquid metals to more than 100,000 for heavy oils by Çengel and Cimbala [2].

1.3.2 Richardson Number

Richardson number represents the importance of natural convection relative to the forced convection. The Richardson number in this context is defined as

$$Ri = \frac{g\beta(T_{hot} - T_{ref})}{V^2}$$

Where g is the gravitational acceleration, β is the thermal expansion coefficient, T_{hot} is the hot wall temperature, T_{ref} is the reference temperature, L is the characteristic length, and V is the characteristic velocity. The Richardson number can also be expressed by using a combination of the Grashof number and Reynolds number,

$$Ri = \frac{Gr}{Re^2}$$

Typically, the natural convection is negligible when $Ri < 0.1$, forced convection is negligible when $Ri > 10$, and neither is negligible when $0.1 < Ri < 10$. It may be noted that usually, the forced convection is large relative to natural convection except in the case of extremely low forced flow velocities. However, buoyancy often plays a significant role in defining the laminar-turbulent transition of a mixed convection flow. In the design of water filled thermal energy storage tanks, the Richardson number can be useful by Çengel and Cimbala [2].

1.3.3 Reynolds Number

The transition from laminar to turbulent flow depends on the surface geometry, surface roughness, flow velocity, surface temperature and type of fluid, among other things. In 1883 Osborn Reynolds discovered that the flow regime depends mainly on the ratio of the inertia forces to friction forces in the fluid. This ratio is called the Reynolds number, which is a dimensionless quantity, and is defined as

$$\begin{aligned}
 Re &= \frac{\textit{inertia Force}}{\textit{Friction Force}} \\
 &= \frac{\textit{Mass} \times \textit{Accelaretion}}{\textit{Shering Stress} \times \textit{Cross sectional Area}} \\
 &= \frac{\textit{Volume} \times \textit{Density} \times (\textit{Velocity} / \textit{Time})}{\mu \times (\textit{Velocity} / \textit{Length}) \times \textit{Cross Sectional Area}} \\
 &= \frac{(\textit{Length})^3 \times \textit{Density} \times (\textit{Length} / \textit{Time})}{\mu \times (\textit{Length})^2} \\
 &= \frac{\textit{Length} \times \textit{Density} \times \textit{Velocity}}{\mu} \\
 &= \frac{L \times \rho \times V}{\mu} \\
 &= \frac{LV}{\mu / \rho} \\
 &= \frac{LV}{\nu}
 \end{aligned}$$

Here V , L , ρ and μ . are characteristic values of reference velocity, characteristic length; density and coefficient of viscosity of the fluid flow respectively and $\nu = \frac{\mu}{\rho}$ is the kinematic viscosity by Çengel and Cimbala [2].

1.3.4 Hartmann Number

Hartmann number is the ratio of electromagnetic force to the viscous force first introduced by Hartmann. It is defined by $Ha = B_0 L \sqrt{\frac{\sigma}{\mu}}$

Where B_0 is the magnetic field, L is the characteristic length scale, σ is the electric conductivity and μ is the viscosity. In addition, it is a dimensionless quantity characterizing the flow of conducting fluid in a transverse magnetic field, being the product of the magnetic flux density, a representative length and the square root of the ratio of electric conductivity to viscosity by Çengel and Cimbala [2].

1.4 MIXED CONVECTION HEAT TRANSFER IN CAVITIES

Mixed convection in cavities is a topic of contemporary importance because cavities filled with fluid are central components in a long list of engineering and geophysical systems. The flow and heat transfer induced in a cavity differs fundamentally from the external mixed convection boundary layer. Mixed convection in a cavity unlike the external mixed convection boundary layer that is caused by the heat transfer interaction between a single wall and a very large fluid reservoir is the result of the complex interaction between finite size fluid systems in thermal communication with all the walls that confine it. The complexity of this internal interaction is responsible for the diversity of flows that can exist inside the cavity. The phenomenon of mixed convection in cavities is varied by the geometry and the orientation of the cavity, judging by the potential engineering applications in Hagen [1]. The cavity phenomena can loosely be organized into two classes.

- Vented cavity and
- Lid-driven cavity

In a vented cavity, where the interaction between the externally forced stream provided by the inlet and the buoyancy-driven flows induced by the heat source leads to the possibility of complex flows. Therefore it is important to understand the fluid flow and heat transfer characteristics of mixed convection in a vented cavity.

On the other hand, the fluid flow and heat transfer in a lid-driven cavity where the flow is induced by a shear force resulting from the motion of a lid combined with the buoyancy force due to non-homogeneous temperature of the cavity wall, provides another problem, studied extensively by researchers to understand the interaction between buoyancy and shearing forces in such flow situation. The interaction between buoyancy driven and shear driven flows inside a closed cavity in a mixed convection regime is quite complex. Therefore it is also important to understand the fluid flow and heat transfer characteristics of mixed convection in a lid-driven cavity.

1.5 LITERATURE REVIEW

Convection heat transfer in a lid-driven cavity has drawn the interest by the researchers because of its wide range of applications such as solar collectors, microelectronic devices, float glass production and electrical components etc.

Many researchers have paid attention to the lid-driven square cavity, both from engineering and theoretical viewpoint. Mahmud et al. [4] Analyzed free convection in an enclosure with vertical wavy walls. They observed that the higher heat transfer at lower aspect ratios for a certain value of the Grashof number. Das and Mahmud [5] have studied natural convection inside a wavy enclosure. Their results illustrated that the amplitude and the number of undulations of the wavy wall affect heat transfer characteristics inside the cavity. Misirlioglu et al. [6] studied numerically natural convection inside an inclined wavy enclosure filled with a porous medium. Al-Amiri et al. [7] investigated the effect of sinusoidal wavy bottom surface on mixed convection heat transfer in a lid-driven cavity. They investigated the effect of Richardson number, undulation number and amplitude of the wavy surface on flow structure and heat transfer characteristics. Rostami [8] numerically simulated the unsteady natural convection in an enclosure with vertical wavy walls. Mansour et al. [9] considered numerically the problem of natural convection in wavy porous cavities under the influence of thermal radiation using a thermal non-equilibrium model. Mushate [10] Analyzed CFD prediction of natural convection in a wavy cavity filled with Porous medium. Also, the results indicated that the rate of heat transfer increases as the Rayleigh number increases and decreases with the increase of amplitude. Abu-Nada and Chamkha [11] numerically simulated the mixed

convection flow of a nanofluid in a lid-driven cavity with a wavy wall. They found that the heat transfer rate increases with the volume fraction of nanoparticles for all values of Richardson numbers and bottom wall geometry ratios. Sheremet and Pop [12] studied the natural convection in a wavy porous cavity with sinusoidal temperature distributions on both side walls filled with a nanofluid: Buongiorno's mathematical model.

Convective flow and heat transfer from wavy surfaces is given by Shenoy et al. [13]. The authors of this book provided an excellent background in the field of natural convection and heat transfer in wavy cavities filled with viscous fluids, porous media, and nanofluids. Recently, Sheremet et al. [14] studied free convection in a partially heated wavy porous cavity filled with a nanofluid under the effects of Brownian diffusion and thermophoresis. Cheong et al. [15] considered the natural convection in a wavy porous cavity with sinusoidal heating and internal heat generation. Alsabery et al. [16] reported the effect of rotating solid cylinder on entropy generation and convective heat transfer in a wavy porous cavity heated from below. They showed that the flow control can be accomplished by the angular rotational velocity or direction of the cylinder rotation. Moreover they seen that, an augmenting in the porosity of the medium causes an increase in heat transfer from the wall to the fluid and therefore an increase in the convective flow and consequently a decrease in the Bejan number.

Magnetic field effect of electrically conducting fluid on the heat transfer and fluid flow encountered in many engineering applications such as purification of molten metal's, MHD power generators, micro MHD pumps and liquid metal flow control etc. Magnetic field effects are also important in medicine. Tumour treating fields are said to be a 4th treatment in the battle against cancer. Doctors inject a magnetically-sensitive fluid into the cancer area and use a powerful magnet to generate heat in the body. The heat kills the cancer cells without harming healthy organs. Vacuum cleaners, blenders and washing machines all have electric motors that work by magnetic principles. Rahman et al. [17] studied the conjugate effect of Joule heating and magnetic force, acting normal to the left vertical wall of an obstructed lid-driven cavity saturated with an electrically conducting fluid numerically using finite

element method. They showed that the Joule heating parameter and the Hartmann number have a notable effect on fluid flow and heat transfer. Saha et al. [18] investigated the effect of internal heat generation or absorption on MHD mixed convection flow in a lid driven cavity. They observed that the heat transfer rate decreases with increasing of Hartmann number and heat generation parameter whereas increases for the increasing values of heat absorption parameter. Thus, the magnetic field plays an important role to control heat transfer and fluid flow. The rate of reduction is higher for high values of the Richardson number. Khudheyer [19] numerically simulated the MHD mixed convection in double lid- driven differentially heated trapezoidal cavity. The results show that at mixed convection regime ($Ri = 1$) and in the absences of the magnetic field ($Ha = 0$), the maximum heat transfer occurs for trapezoidal cavity at inclined wall angle (30^0). Ali et al. [20] studied the magnetohydrodynamic mixed convection flow in a hexagonal enclosure. They found that Hartmann number and Richardson number have a considerable effect on the flow field and temperature field. Öztop et al. [21] Analyzed mixed convection of MHD flow in nanofluid filled and partially heated wavy walled lid-driven enclosure. They showed that the rate of heat transfer decreases with increasing the Hartmann number. The rate of heat transfer can be enhanced or reduced by increasing the volume fraction of nanoparticles based on Hartmann and Richardson numbers. Ashorynejad and Shahriari [22] studied the MHD natural convection of hybrid nanofluid in an open wavy cavity.

Additionally, due to various engineering applications of the problem of fluid flow and heat transfer inside the enclosure with a fin such as radiators in cars, computer CPU heat sinks, heat exchangers in power plants and heat exchanging devices. They are also used in newer technology such as hydrogen fuel cells. Frederick [23] studied numerically natural convection in an inclined square enclosure with a partition attached to its cold wall. Bilgen [24] studied numerically natural convection in cavities with a thin fin on the hot wall. It was found that the heat transfer rate was a lower limit with the fin attached to the middle of near the middle of the heated wall. Shi and Khodadadi [25] investigated the steady laminar natural convection heat transfer in a differentially heated square cavity due to a thin fin on the hot wall. They found that for higher value Rayleigh number, the heat transfer rate

was enhanced irrespective of the fin position or length. Frederick and Valencia [26] studied numerically heat transfer in a square cavity with a conducting partition on its hot wall. It was found that increasing thermal conductivity ratio enhanced heat transfer. Nag et al. [27] studied numerically natural convection in a differentially heated square cavity with horizontal partition plate on the hot wall. The study was done for two cases: a highly conductive fin and an adiabatic fin. For the case of a highly conductive fin, it was found that the Nusselt number on the cold wall increased compared to the case with no fin. For the case with the adiabatic fin, heat transfer was reduced compared to the case without a fin. Bilgen [28] studied natural convection in enclosures with partial partitions. It was concluded that up to $Ra = 10^8$, laminar flow regime was found while turbulent flow regime starts to be formed for higher values of Rayleigh number. Shi and Khodadadi [29] investigated the steady laminar fluid flow and heat transfer in a lid-driven cavity due to a thin fin. They concluded that the fin slowed the flow near the anchoring wall and reduces the temperature gradient, thus the heat transfer capacity was degraded. Three-dimensional study of natural convection for air inside a cubic enclosure with a thick fin attached to the hot left wall was conducted by Frederick and Moraga [30] studied the three-dimensional natural convection in finned cubical enclosures. The study showed that by increasing the thermal conductivity ratio between the fin material and the air inside the enclosure, the cell was displaced away from the hot wall and the blockage effect was reduced. They also found that for a high conductivity ratio, 20% enhancement of heat transfer was obtained compared to the cube without a fin. Tasnim and Collins [31] investigated numerically natural convection heat transfer in a square cavity with a baffle on hot wall. They found that the effect of fin position on the heat transfer rate was depended strongly affected by Rayleigh number and the fin length. Öztop and Bilgen [32] studied numerically natural convection in differentially heated and partially divided square cavities with internal heat generation. The study has shown that increasing both the thickness and length of the cold partition reduce the heat transfer rate. Ben-Nakhi and Chamkha [33] reported the effect of length and inclination of a thin fin on natural convection in a square enclosure. It was found that the effect of fin inclination angle was dependent on the fin length. Ben-Nakhi and Chamkha [34] also studied numerically conjugate natural

convection in a square enclosure with inclined thin fin of arbitrary length. They found that increasing the thermal conductivity and decreasing the fin length enhanced the average Nusselt number on the hot wall while increasing the fin length enhanced the average Nusselt number on cold surfaces. Sun et al. [35] studied numerically mixed convection in lid-driven enclosures using conductive triangular fins. They observed that the triangular fin is a good control parameter for flow structure, temperature field and rate of heat transfer. Dariz et al. [36] investigated the fin effect on mixed convection heat transfer in a lid-driven cavity. Heat transfer was observed for the cavity with fewer fins and high Richardson number. Xu et al. [37] reported the effect of the fin length on natural convection flow transition in a cavity. They found that the flow near the finned wall changes from a steady to periodic unsteady flow at a critical Rayleigh number that is sensitive to the fin length. Xu and Saha [38] studied the transition to an unsteady flow induced by a fin on the sidewall of a differentially heated air-filled square cavity and heat transfer. Elatar et al. [39] performed a numerical study on laminar natural convection inside square enclosure with adiabatic horizontal wall with a single horizontal fin at different length and positions attached to the hot wall. They investigated the effect of Rayleigh number, fin lengths and fin positions of the enclosure on fluid flow structure and heat transfer characteristics. Gdhaidh et al. [40] investigated analytically the enhancement of natural convection heat transfer within closed enclosure using parallel fins. They observed that as the fin number increases the maximum heat source temperature decreases.

1.6 PARTICULAR APPLICATIONS

Mixed convection heat transfer has always been of great interest because of its wide range of applications. The relevant research output has numerous applications such as MHD power generators, radiators in cars, computer CPU heat sinks, hydrogen fuel cells, biological transportation, geophysical fluid mechanics, liquid metal flow control and etc. Magnetic field effects are also important in medicine. Tumors treating fields are said to be a 4th treatment in the battle against cancer.

1.7 OBJECTIVES OF THE PRESENT STUDY

A review of earlier studies indicates that the mixed convection heat transfer in presence of magnetic field in a lid-driven wavy cavity having vertical fin has not been analyzed yet. The study will be carried out numerically with an accurate numerical procedure, and the related results will be shown using streamlines, isotherms, and related graphs and charts.

1.7.1 Objectives with Specific Aims

The specific objectives of the present research work are to:

- 1) Analyze the variation of heat transfer due to vertical heated fin attached to the bottom wall of the cavity having wavy side walls.
- 2) Investigate the effects of physical parameters such as Richardson number (Ri), and Hartmann number (Ha) on the flow field inside the cavity with appropriate boundary conditions.
- 3) Investigate the effects of the fin lengths on the flow field and temperature distribution.

1.7.2 Possible Outcome

The outcomes of the study are

- 1) The flow structure inside the enclosure expected to be noticeably affected by the variation of fin position and length. The heat transfer rate could be enhanced for greater Richardson number (Ri) with lower Hartmann number (Ha).
- 2) The strength of magnetic field and isotherms are might be affected by the increase of the Richardson number.
- 3) The velocity magnitude might decline with the increase of Hartmann number (Ha) while the same value of Richardson number (Ri).
- 4) The results can be helpful in a wide range of applications including renewable energy, solar collectors, cooling of nuclear reactors, liquid metal flow control, electrical components, biological transportation and so on.

1.8 OUTLINE OF THE THESIS

This dissertation contains five chapters. In chapter 1, a brief introduction is presented with aim and objective. This chapter also consists of a literature review of the past studies on fluid flow and heat transfer in cavities. In this state-of-the-art review, different aspects of the previous studies have been mentioned categorically. This is followed by the post-mortem of a recent historical event for the illustration of fluid flow and heat transfer effects in cavities or wavy enclosure having fin.

In Chapter 2 we have discussed the computational technique of the problem for viscous incompressible flow.

In Chapter 3 mixed convection heat transfer in presence of magnetic field in a lid-driven wavy cavity having vertical fin have been investigated numerically. Mathematical modeling and Finite Element Formulation is employed in this study and explained elaborately.

In Chapter 4 a detailed parametric study on mixed convection heat transfer in presence of magnetic field in a lid-driven wavy cavity having vertical fin is conducted. Effects of the major parameters such as Richardson number, Hartmann number and the physical parameter such fin length on the flow and thermal field with cavity have been presented.

Finally, in Chapter 5 the dissertation is rounded off with the conclusions. Lastly, recommendations for further study of the present problem are outlined.

CHAPTER 2

COMPUTATIONAL TECHNIQUE

Computational fluid dynamics (CFD) has been rapidly gaining popularity over the past several years for technological as well as scientific interests. For many problems of industrial interest, experimental techniques are extremely expensive or even impossible due to the complex nature of the flow configuration. Analytical methods are often useful in studying the basic physics involved in a certain flow problem, however, in many interesting problems; these methods have limited direct applicability. The dramatic increase in computational power over the past several years has led to a heightened interest in numerical simulations as a cost-effective method of providing additional flow information, not readily available from experiments, for industrial applications, as well as a complementary tool in the investigation of the fundamental physics of turbulent flows, where analytical solutions have so far been unattainable. It is not expected (or advocated), however, that numerical simulations replace theory or experiment, but that they are used in conjunction with these other methods to provide a more complete understanding of the physical problem at hand.

Mathematical model of physical phenomena may be ordinary or partial differential equations, which have been the subject of analytical and numerical investigations. The partial differential equations of fluid mechanics and heat transfer are solvable for only a limited number of flows. To obtain an approximate solution numerically, we have to use a discretization method, which approximated the differential equations by a system of algebraic equations, which can then be solved on a computer. The approximations are applied to small domains in space and/or time so the numerical solution provides results at discrete locations in space and time. Much as the accuracy of experimental data depends on the quality of the tools used, the accuracy of numerical solutions depend on the quality of discretizations used. Computational fluid dynamics (CFD) computation involves the formation of a set number that constitutes a practical approximation of a real-life system. The outcome of the computation process improves the understanding of the performance of a system. Thereby, engineers need CFD codes that can make physically realistic results with

good quality accuracy in simulations with finite grids. Contained within the broad field of computational fluid dynamics are activities that cover the range from the automation of well-established engineering design methods to the use of detailed solutions of the Navier-Stokes equations as substitutes for experimental research into the nature of complex flows. CFD has been used for solving a wide range of fluid dynamics problem. It is more frequently used in fields of engineering where the geometry is complicated or some important feature that cannot be dealt with standard methods. More details are available in Ferziger & Perić [41] and Patankar [42].

The remainder of this chapter, a tutorial introduction to the computational method with advantages of numerical investigation because the numerical method has played a central role in this thesis. Various components of the numerical method have been also explained. Finally, the major steps involved in finite element analysis of a typical problem have been discussed.

2.1 MERITS AND DEMERITS OF NUMERICAL METHOD

As computational power grows, the need for more advanced numerical algorithms also increases. There are many different techniques for constructing numerical solutions of fluid flow problems, e.g. finite difference methods (FD), finite volume methods (FV), and finite element methods (FE), to name a few, and all have their strengths and weaknesses. Since the goal of the present research lies in the development of methods which may ultimately be used for large-scale applications of industrial interest, finite element methods have been chosen, given their accuracy as well as their ability to approximate arbitrarily complex geometric configurations. The finite element method applied to fluid dynamics has reached a level of maturity over the past two decades such that it is now being successfully applied to industrial strength problems including turbulent flows. More details are available in Ferziger & Perić [41] and Patankar [42].

Finite element method is an ideal numerical approach for solving a system of partial differential equations. The finite element method produces equations for each element independently of all other elements. Only when the equations are collected together and assembled into a global matrix are the interactions between elements

taken into account. Despite these ideal characteristics, the finite element method dominates in most of the computational fluid dynamics. The present research is an attempt to bring the FE technique again into light through a novel formulation of two-dimensional incompressible thermal flow problems. As the formulation establishes a priority of finite element technique over the FD and FV method, the philosophy and approach of the three methods are recapitulated here in brief. The finite difference method relies on the philosophy that the body is in one single piece but the parameters are evaluated only at some selected points within the body, satisfying the governing differential equations approximately, whereas the finite volume method relies on the philosophy that the body is divided into a finite number of control volumes, On the other hand, in the finite element method, the body is divided into a number of elements. The Finite element method works when all other methods fail and it's managing complex geometrical bodies and boundaries. There are many commercial packages such as ANSYS, MATLAB and COMSOL MULTIPHYSICS for analyzing practical problems. The demerits of this method, it considers the body is not in one piece, but it is an assemblage of elements connected only at nodes and Finite element solution is highly dependent on the element type.

Accurate and reliable prediction of complex geometry is of great importance to meet the severe demand of greater reliability as well as an economic challenge. It is noted that these complex geometries occur most frequently in CFD. Presented methods have a common feature: they generate equations for the values of the unknown functions at a finite number of points in the computational domain. But there are also several differences. The finite difference and the finite volume methods generate numerical equations at the reference point based on the values at neighbouring points. The finite element method takes care of boundary conditions of Neumann type while the other two methods can easily apply to the Dirichlet conditions. The finite difference method could be easily extended to multidimensional spatial domains if the chosen grid is regular (the cells must look cuboids, in a topological sense). The grid indexing is simple but some difficulties appear for the domain with complex geometry. For the finite element method, there are no restrictions on the connection of the elements when the sides (or faces) of the elements are correctly aligned and have the same nodes for the neighbouring elements. This flexibility

allows us to model very complex geometry. The finite volume method could also use irregular grids like the grids for the finite element methods but keeps the simplicity of writing the equations like that for the finite difference method. Of course, the presence of a complex geometry slows down the computational programs. Another benefit of the finite element method is that of the specific mode to deduce the equations for each element that are then assembled. Therefore, the addition of new elements by a refinement of the existing ones is not a major problem. For the other methods, the mesh refinement is a major task and could involve the rewriting of the program. But for all the methods used for the discrete analogue of the initial equation, the obtained system of simultaneous equations must be solved. That is why the present work emphasizes the use of finite element techniques to solve flow and heat transfer problems. The details of this method are explained in the following section.

2.2 ELEMENTS OF NUMERICAL SOLUTION METHODS

Several components of numerical solution methods are available in Ferziger and Perić [41], here only the main steps will be demonstrated in the following.

2.2.1 Mathematical Model

The starting point of any numerical method is the mathematical model, i.e. the set of partial differential equations and boundary conditions. A solution method is usually designed for a particular set of equations. Trying to produce a general-purpose solution method, i.e. one which is applicable to all flows, is impractical, if not impossible and as with most general purpose tools, they are usually not optimum for any one application.

2.2.2 Discretization Process

After selecting the mathematical model, one has to choose a suitable discretization method, i.e. a method of approximating the differential equations by a system of algebraic equations for the variable at some set of discrete locations in space and time by Ferziger and Perić [41].

2.2.3 Numerical Grid

The numerical grid defines the discrete locations, at which the variables are to be calculated, which is essentially a discrete representation of the geometric domain on which the problem is to be solved. It divided the solution domain into a finite number of sub-domains (elements, control volumes etc). Some of the options available are a structural (regular) grid, block-structured grid, unstructured grids etc.

2.2.4 Finite Approximations

Following the choice of grid type, one has to select the approximations to be used in the discretization process. In a finite difference method, approximations for the derivatives at the grid points have to be selected. In a finite volume method, one has to select the methods of approximating surface and volume integrals. In a finite element method, one has to choose the functions and weighting functions.

2.2.5 Solution Technique

Discretization yields a large system of non-linear algebraic equations. The method of solution depends on the problem. For unsteady flows, methods based on those used for initial value problems for ordinary differential equation (marching in time) is used. At each time step, an elliptic problem has to be solved. Pseudo-time marching or equivalent iteration schemes usually solve steady flow problems. Since the equations are non-linear, an iteration scheme is used to solve them. These methods use successive linearization of the equations and the resulting linear systems are almost always solved by iterative techniques. The choice of solver depends on the grid type and the number of nodes involved in each algebraic equation. More details are available in Patankar [42].

2.3 DISCRETIZATION APPROACHES

The first step to numerically solve a mathematical model of physical phenomena is its numerical discretization. This means that each component of the differential equations is transformed into a “numerical analogue” which can be represented in the computer and then processed by a computer program, built on some algorithm by Ferziger & Perić [41] and Patankar [42].

There are several discretization methods available for the high-performance numerical computation in CFD are given below.

- Finite volume method (FVM)
- Finite element method (FEM)
- Finite difference method (FDM)
- Boundary element method (BEM)
- Boundary volume method (BVM)

In the present numerical computation, the Galerkin finite element method (FEM) has been used.

2.4 FINITE ELEMENT METHOD

The finite element method (FEM) is a powerful computational technique for solving problems which are described by partial differential equations or can be formulated as functional minimization. The basic idea of the finite element method is to view a given domain as an assemblage of simple geometric shapes, called finite elements, for which it is possible to systematically generate the approximation functions needed in the solution of partial differential equations by the variational or weighted residual method. The computational domains with irregular geometries by a collection of finite elements make the method a valuable practical tool for the solution of the boundary layer, initial and eigenvalue problems arising in various fields of engineering.

The approximation functions, which satisfy the governing equations and boundary conditions, are often constructed using ideas from interpolation theory. Approximating functions in finite elements are determined in terms of nodal values of a physical field which is sought. A continuous physical problem is transformed into a discretized finite element problem with unknown nodal values. For a linear problem, a system of linear algebraic equations should be solved. Values inside finite elements can be recovered using nodal values. More details are available in by Taylor & Hood [43] and Dechaumphai [44].

The major steps involved in finite element analysis of a typical problem are:

1. Discretization of the domain into a set of finite elements (mesh generation).
2. Weighted-integral or weak formulation of the differential equation to be analyzed.
3. Development of the finite element model of the problem using its weighted-integral or weak form.
4. Assembly of finite elements to obtain the global system of algebraic equations.
5. Imposition of boundary conditions.
6. Solution of equations.
7. Post-computation of solution and quantities of interest.

2.4.1 Mesh Generation

The present numerical technique will discretize the computational domain into unstructured triangles by Delaunay Triangular method. The Delaunay triangulation is a geometric structure that has enjoyed great popularity in mesh generation since the mesh generation was in its infancy. In two dimensions, the Delaunay triangulation of a vertex set maximizes the minimum angle among all possible triangulations of that vertex set. Figure 2.1 shows the mesh mode for the present numerical computation. Mesh generation has been done meticulously.

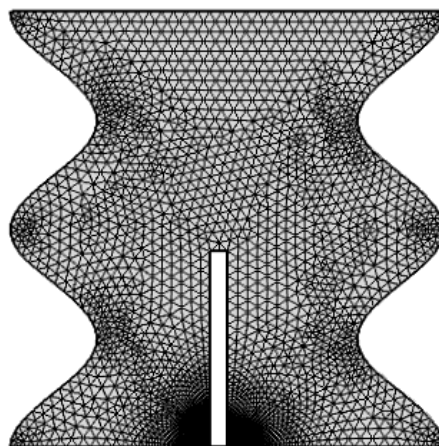


Figure 2.1: Current mesh structure of elements for wavy cavity with fin length $L = 0.45$, fin position $D = 0.50$, fin thickness $B = 0.04$, $A = 0.1$ and $\lambda = 2$

2.4.2 Computational Technique

Discretization yields a large system of non-linear algebraic equations. The method of solution depends on the problem. For unsteady flows, methods based on those used for initial value problems for ordinary differential equation (marching in time) is used. At each time step an elliptic problem has to be solved. Pseudo-time marching or an equivalent iteration scheme usually solves steady flow problems. Since the equations are non-linear, an iteration scheme is used to solve them. These methods use successive linearization of the equations and the resulting linear systems are almost always solved by iterative techniques. The choice of solver depends on the grid type and the number of nodes involved in each algebraic equation.

2.5 ALGORITHM

The algorithm was originally put forward by the iterative Newton-Raphson algorithm; the discrete forms of the continuity, momentum and energy equations are solved to find out the value of the velocity and the temperature. It is essential to guess the initial values of the variables. Then the numerical solutions of the variables are obtained while the convergent criterion is fulfilled. The simple algorithm is shown by the flow chart below.

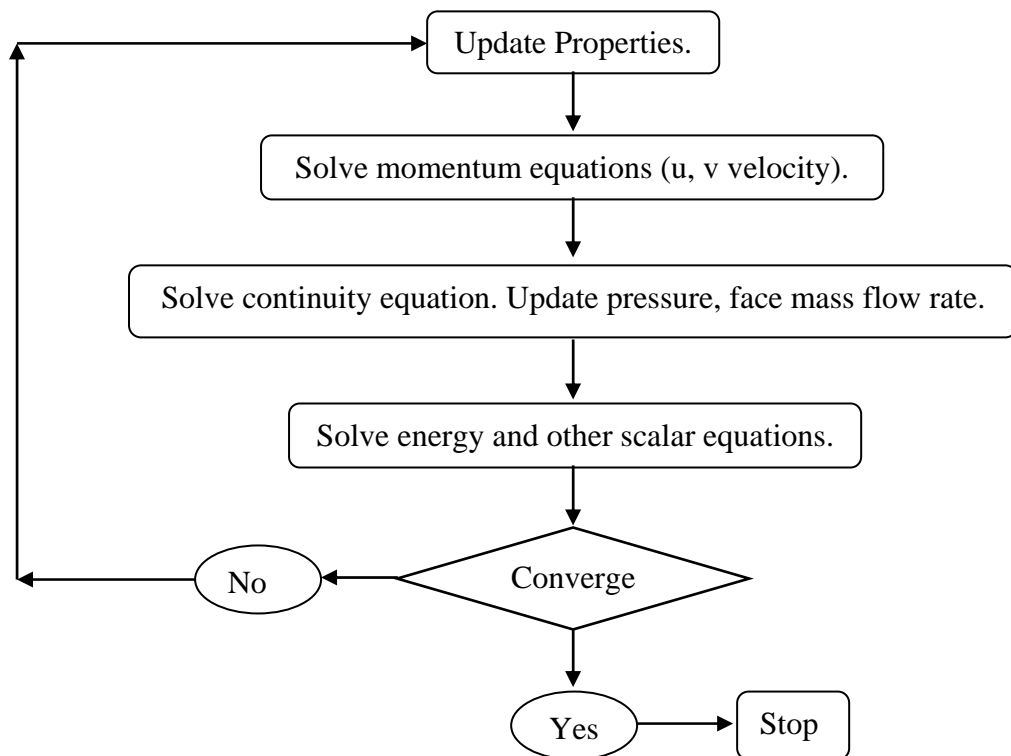


Figure 2.2: Flow chart of the computational procedure

2.5.1 Solution of System of Equations

A system of linear algebraic equations has been solved by the UMFPACK with MATLAB interface. UMFPACK is a set of routines for solving asymmetric sparse linear systems $Ax = b$, using the Asymmetric MultiFrontal method and direct sparse LU factorization by Taylor and Hood [43] and Dechaumphai [44]. Five primary UMFPACK routines are required to factorize A or $Ax = b$:

1. Pre-orders the columns of A to reduce fill-in and performs a symbolic analysis.
2. Numerically scales and then factorizes a sparse matrix.
3. Solves a sparse linear system using the numeric factorization.
4. Frees the Symbolic object.
5. Frees the Numeric object.

Additional routines are:

1. Passing a different column ordering
2. Changing default parameters
3. Manipulating sparse matrices
4. Getting LU factors
5. Solving the LU factors
6. Computing determinant

UMFPACK factorizes PAQ , $PRAQ$, or $PR^{-1}AQ$ into the product LU , where L and U are lower and upper triangular, respectively, P and Q are permutation matrices, and R is a diagonal matrix of row scaling factors (or $R = I$ if row-scaling is not used). Both P and Q are chosen to reduce fill-in (new nonzeros in L and U that are not present in A). The permutation P has the dual role of reducing fill-in and maintaining numerical accuracy (via relaxed partial pivoting and row interchanges). The sparse matrix A can be square or rectangular, singular or non-singular, and real or complex (or any combination). Only square matrices A can be used to solve $Ax = b$ or related systems. Rectangular matrices can only be factorized. UMFPACK first finds a column pre-ordering that reduces fill-in, without regard to numerical values. It scales and analyzes the matrix, and then automatically selects one of three strategies for pre-

ordering the rows and columns: asymmetric, 2-by-2 and symmetric. These strategies are described below.

One notable attribute of the UMFPACK is that whenever a matrix is factored, the factorization is stored as a part of the original matrix so that further operations on the matrix can reuse this factorization. Whenever a factorization or decomposition is calculated, it is preserved as a list (element) in the factor slot of the original object. In this way, a sequence of operations, such as determining the condition number of a matrix and then solving a linear system based on the matrix, do not require multiple factorizations of the intermediate results.

Conceptually, the simplest representation of a sparse matrix is as a triplet of an integer vector \mathbf{i} giving the row numbers, an integer vector \mathbf{j} giving the column numbers, and a numeric vector \mathbf{x} giving the non-zero values in the matrix. The triplet representation is row-oriented if elements in the same row were adjacent and column-oriented if elements in the same column were adjacent. The compressed sparse row (CSR) or compressed sparse column (CSC) representation is similar to a row-oriented triplet or column-oriented triplet respectively. These compressed representations remove the redundant row or column in indices and provide faster access to a given location in the matrix.

CHAPTER 3

MATHEMATICAL MODELLING

The convection heat transfer occurs due to temperature difference that affects the density and thus relative buoyancy of the fluid which is referred to as combined or mixed convection. The starting point of any numerical method is the mathematical model, i.e. the set of partial differential equations and boundary conditions. A solution method is usually designed for a particular set of equations. Trying to produce a general-purpose solution method, i.e. one which is applicable to all flows, is impractical, if not impossible and as with most general purpose tools, they are usually not optimum for any one application. The generalized governing equations are used based on the conservation laws of mass, momentum and energy. As the heat transfer depends upon a number of factors, dimensional analysis is presented to show the important non-dimensional parameters which will influence the dimensionless heat transfer parameter.

The remainder of this chapter is as follows. In section 3.1, the physical configurations of the current research interest are shown. Then the appropriate mathematical model (both governing equations and boundary conditions) is considered in section 3.2. After that, a numerical scheme that is employed in this study is described in section 3.3.

3.1 PHYSICAL CONFIGURATIONS

A wavy cavity is considered for the present study with physical configuration and boundary conditions as shown in Fig. 3.1 which represents of the two-dimensional lid-driven wavy cavity of height and width W . The top and bottom walls are kept at a constant heat temperature (T_h) whereas the vertical wavy walls are kept at a constant cold temperature (T_c) maintaining $T_h > T_c$. A heated fin of length (l) and thickness (b) is attached to the hot bottom wall at a position (d) from the base of the left wavy wall. The top wall moves from right to left with constant velocity. The gravitational force acts in the vertically downward direction and uniform magnetic field with a constant magnitude (B_0) in the direction of the moving lid is applied.

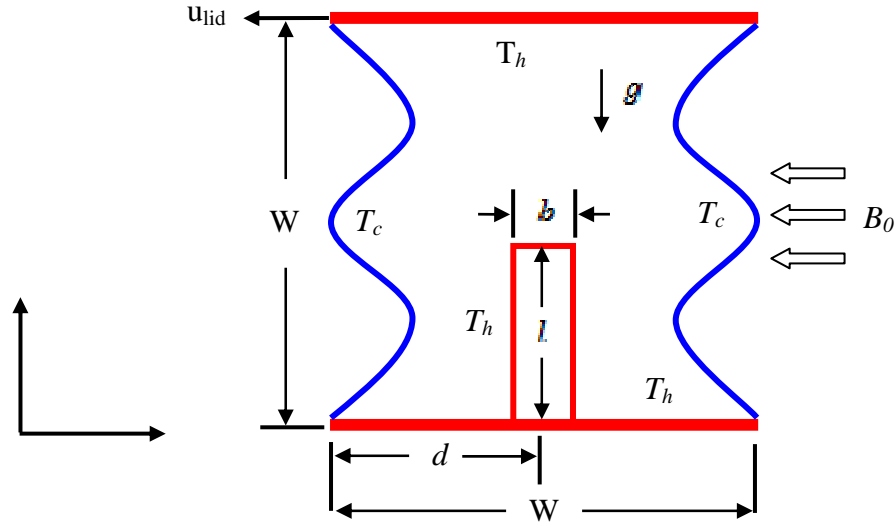


Figure 3.1: Schematic diagram of the wavy cavity with boundary conditions

3.2 GOVERNING EQUATIONS ALONG WITH BOUNDARY CONDITIONS

The fundamental laws used to solve the fluid flow problems are the law of conservation of mass or continuity equations, conservation of momentum, and conservation of energy, which constitute a set of coupled, nonlinear, partial differential equations. The thermo-physical properties of the fluid are assumed to be constant, except for the density variation in the buoyancy term which is treated according to Boussinesq approximation while the effects of radiation and non-viscous dissipation are neglected. In general, the enclosure fluid is assumed to be Newtonian and incompressible, steady and laminar flow.

Following the previous assumptions, the system of equations governing the two-dimensional form as follows:

Continuity Equation

$$\frac{\partial u}{\partial x} + \frac{\partial v}{\partial y} = 0 \quad (3.1)$$

Momentum Equations

$$u \frac{\partial u}{\partial x} + v \frac{\partial u}{\partial y} = -\frac{1}{\rho} \frac{\partial p}{\partial x} + \nu \left(\frac{\partial^2 u}{\partial x^2} + \frac{\partial^2 u}{\partial y^2} \right) \quad (3.2)$$

$$u \frac{\partial v}{\partial x} + v \frac{\partial v}{\partial y} = -\frac{1}{\rho} \frac{\partial p}{\partial y} + \nu \left(\frac{\partial^2 v}{\partial x^2} + \frac{\partial^2 v}{\partial y^2} \right) + g\beta(T - T_c) - \frac{\sigma B_0^2}{\rho} v \quad (3.3)$$

Energy Equations

$$u \frac{\partial T}{\partial x} + v \frac{\partial T}{\partial y} = \alpha \left(\frac{\partial^2 T}{\partial x^2} + \frac{\partial^2 T}{\partial y^2} \right) \quad (3.4)$$

where u and v are the velocity components along x -axis and y -axis respectively, p is the pressure, ρ is the density, ν is the kinematic viscosity, g is the acceleration due to gravitational, β is the volumetric thermal expansion coefficient, σ is the electrical conductivity, B_0 is the magnitude of Magnetic field, T is the temperature and $\alpha = \frac{k}{\rho c_p}$ is the thermal diffusivity.

3.2.1 Dimensional Boundary Conditions

No-slip boundary conditions are used and problems are specified as follows:

On the top wall: $u = u_{lid}, v = 0, T = T_h$

On the bottom wall: $u = v = 0, T = T_h$

On the left vertical wavy wall: $u = v = 0, T = T_c; A(1 - \cos(2\pi\lambda y))$

On the right vertical wavy wall: $u = v = 0, T = T_c; 1 - A(1 - \cos(2\pi\lambda y))$

For the Fin surface: $0 \leq y \leq l, u = v = 0, T = T_h; x = d + \frac{b}{2}$ and $x = d - \frac{b}{2}$

where A is the amplitude and λ is the number of oscillations.

3.2.2 Dimensional Analysis

The non-dimensional parameters that are used for making the governing equations (3.1–3.4) into dimensionless form are stated as follows:

$$X = \frac{x}{W}, Y = \frac{y}{W}, U = \frac{u}{u_{lid}}, V = \frac{v}{u_{lid}}, P = \frac{p}{\rho u_{lid}^2}, \theta = \frac{T - T_c}{T_h - T_c}, H = \frac{h}{W}, L = \frac{l}{W} \text{ and } B = \frac{b}{W}$$

where X and Y are the coordinates varying along with horizontal and vertical directions, respectively, U and V are, the velocity components in the X and Y directions, respectively, θ is the dimensionless temperature and P is the dimensionless pressure. After substitution the dimensionless variables into the equations (3.1-3.4), we get the following dimensionless equations as

Continuity Equation

$$\frac{\partial U}{\partial X} + \frac{\partial V}{\partial Y} = 0 \quad (3.5)$$

Momentum Equations

$$U \frac{\partial U}{\partial X} + V \frac{\partial U}{\partial Y} = -\frac{\partial P}{\partial X} + \frac{1}{Re} \left(\frac{\partial^2 U}{\partial X^2} + \frac{\partial^2 U}{\partial Y^2} \right) \quad (3.6)$$

$$U \frac{\partial V}{\partial X} + V \frac{\partial V}{\partial Y} = -\frac{\partial P}{\partial Y} + \frac{1}{Re} \left(\frac{\partial^2 V}{\partial X^2} + \frac{\partial^2 V}{\partial Y^2} \right) + Ri \theta - \frac{Ha^2}{Re} V \quad (3.7)$$

Energy Equations

$$U \frac{\partial \theta}{\partial X} + V \frac{\partial \theta}{\partial Y} = \frac{1}{Re Pr} \left(\frac{\partial^2 \theta}{\partial X^2} + \frac{\partial^2 \theta}{\partial Y^2} \right) \quad (3.8)$$

The non-dimensional numbers that appear in equations (3.6) - (3.8) are as follows:

$$Pr = \frac{\nu}{\alpha}, Re = \frac{u_{lid} W}{\nu}, Gr = \frac{g \beta (T_h - T_c) W^3}{\nu^2}, Ha = B_0 W \sqrt{\frac{\sigma}{\mu}} \text{ and } Ri = \frac{Gr}{Re^2}$$

3.2.3 Boundary Conditions (non-dimensional)

On the top wall: $U = -1, V = 0, \theta = 1$

On the bottom wall: $U = V = 0, \theta = 1$

On the left vertical wavy wall: $U = V = 0, \theta = 0; A(1 - \cos(2\pi\lambda Y)), 0 \leq Y \leq 1$

On the right vertical wavy wall: $U = V = 0, \theta = 0; 1 - A(1 - \cos(2\pi\lambda Y)), 0 \leq Y \leq 1$

For the Fin surface: $0 \leq Y \leq L, U = V = 0, \theta = 1; X = D + \frac{B}{2}$ and $X = D - \frac{B}{2}$

where A is the amplitude and λ is the number of oscillations.

3.2.4 Nusselt Number

First, the heat transfer by conduction was equated to the heat transfer by convection

$$h^* \Delta T = -k \frac{\partial T}{\partial n} \quad (3.9)$$

where n is the non-dimensional distances either along x or y -direction acting normal to the surface. By introducing the dimensionless variables into equation (3.9) the local Nusselt number is defined as:

$$Nu_L = - \left. \frac{\partial \theta}{\partial N} \right|_{Surface} \quad (3.10)$$

The average Nusselt number on the cold wall is obtained as follows:

$$Nu_{av} = - \int_0^1 \left. \frac{\partial \theta}{\partial N} \right|_{Surface} dS \quad (3.11)$$

3.3 NUMERICAL ANALYSIS

The governing equations along with the boundary conditions are solved numerically, employing Galerkin weighted residual finite element techniques discussed below.

3.3.1 Finite Element Formulation and Computational Procedure

To derive the finite element equations, the method of weighted residuals Taylor and Hood [43] and Dechaumphai [44] is applied to the equations (3.5) – (3.8) as

$$\int_A N_\alpha \left(\frac{\partial U}{\partial X} + \frac{\partial V}{\partial Y} \right) dA = 0 \quad (3.12)$$

$$\int_A N_\alpha \left(U \frac{\partial U}{\partial X} + V \frac{\partial U}{\partial Y} \right) dA = - \int_A H_\lambda \left(\frac{\partial P}{\partial X} \right) dA + \frac{1}{Re} \int_A N_\alpha \left(\frac{\partial^2 U}{\partial X^2} + \frac{\partial^2 U}{\partial Y^2} \right) dA \quad (3.13)$$

$$\begin{aligned} \int_A N_\alpha \left(U \frac{\partial V}{\partial X} + V \frac{\partial V}{\partial Y} \right) dA &= - \int_A H_\lambda \left(\frac{\partial P}{\partial Y} \right) dA + \frac{1}{Re} \int_A N_\alpha \left(\frac{\partial^2 V}{\partial X^2} + \frac{\partial^2 V}{\partial Y^2} \right) dA \\ + Ri \int_A N_\alpha \theta dA - \frac{Ha^2}{Re} \int_A N_\alpha V dA \end{aligned} \quad (3.14)$$

$$\int_A N_\alpha \left(U \frac{\partial \theta}{\partial X} + V \frac{\partial \theta}{\partial Y} \right) dA = \frac{1}{Re Pr} \int_A N_\alpha \left(\frac{\partial^2 \theta}{\partial X^2} + \frac{\partial^2 \theta}{\partial Y^2} \right) dA \quad (3.15)$$

where A is the element area, N_α ($\alpha = 1, 2, \dots, 6$) is the element interpolation functions for the velocity components and the temperature and H_λ ($\lambda = 1, 2, 3$) is the element interpolation functions for the pressure.

Then apply Gauss's theorem into equations (3.13) - (3.15) to generate the boundary integral terms associated with the surface tractions and heat flux. After that the equations (3.13) - (3.15) become,

$$\int_A N_\alpha \left(U \frac{\partial U}{\partial X} + V \frac{\partial U}{\partial Y} \right) dA + \int_A H_\lambda \left(\frac{\partial P}{\partial X} \right) dA - \frac{1}{Re} \int_A \left(\frac{\partial N_\alpha}{\partial X} \frac{\partial U}{\partial X} + \frac{\partial N_\alpha}{\partial Y} \frac{\partial U}{\partial Y} \right) dA \quad (3.16)$$

$$= \int_{S_0} N_\alpha S_x dS_0$$

$$\int_A N_\alpha \left(U \frac{\partial V}{\partial X} + V \frac{\partial V}{\partial Y} \right) dA + \int_A H_\lambda \left(\frac{\partial P}{\partial Y} \right) dA - \frac{1}{Re} \int_A \left(\frac{\partial N_\alpha}{\partial X} \frac{\partial V}{\partial X} + \frac{\partial N_\alpha}{\partial Y} \frac{\partial V}{\partial Y} \right) dA \quad (3.17)$$

$$- Ri \int_A N_\alpha \theta dA + \frac{Ha^2}{Re} \int_A N_\alpha V dA = \int_{S_0} N_\alpha S_y dS_0$$

$$\int_A N_\alpha \left(U \frac{\partial \theta}{\partial X} + V \frac{\partial \theta}{\partial Y} \right) dA + \frac{1}{Re Pr} \int_A \left(\frac{\partial N_\alpha}{\partial X} \frac{\partial \theta}{\partial X} + \frac{\partial N_\alpha}{\partial Y} \frac{\partial \theta}{\partial Y} \right) dA = \int_{S_w} N_\alpha q_{1w} dS_w \quad (3.18)$$

The equations (3.16) - (3.17) specify surface tractions (S_x , S_y) along outflow boundary S_0 and (3.18) specifying velocity components and fluid temperature or heat flux (q_w) that flows into or out from domain along wall boundary S_w .

The basic unknowns for the above differential equations are the velocity components U , V the temperature, θ and the pressure, P . The six node triangular element is used in this work for the development of the finite element equations. All six nodes are associated with velocities as well as temperature; only the corner nodes are associated with pressure. This means that a lower order polynomial is chosen for pressure and which is satisfied through the continuity equation.

The velocity component and the temperature distributions and linear interpolation for the pressure distribution according to their highest derivative orders in the differential equations (3.5) - (3.8) as

$$U(X, Y) = N_\beta U_\beta \quad (3.19)$$

$$V(X, Y) = N_\beta V_\beta \quad (3.20)$$

$$\theta(X, Y) = N_\beta \theta_\beta \quad (3.21)$$

$$P(X, Y) = H_\lambda P_\lambda \quad (3.22)$$

where $\beta = 1, 2, \dots, 6$; $\lambda = 1, 2, 3$.

Substituting the element velocity component distributions, the temperature distribution, and the pressure distribution from equations (3.19) - (3.22), we get the following equations:

$$\int_A N_\alpha (N_{\beta,x} U_\beta + N_{\beta,y} V_\beta) dA = 0 \quad (3.23)$$

$$\begin{aligned} & \int_A N_\alpha \left[(N_\beta U_\beta)(N_{\gamma,x} U_\gamma) + (N_\beta V_\beta)(N_{\gamma,y} U_\gamma) \right] dA + \int_A H_\lambda H_{\mu,x} P_\mu dA - \\ & \frac{1}{Re} \int_A (N_{\alpha,x} N_{\beta,x} U_\beta + N_{\alpha,y} N_{\beta,y} U_\beta) dA = \int_{S_0} N_\alpha S_x dS_0 \end{aligned} \quad (3.24)$$

$$\begin{aligned} & \int_A N_\alpha \left[(N_\beta U_\beta)(N_{\gamma,x} V_\gamma) + (N_\beta V_\beta)(N_{\gamma,y} V_\gamma) \right] dA + \int_A H_\lambda H_{\mu,y} P_\mu dA - \\ & \frac{1}{Re} \int_A (N_{\alpha,x} N_{\beta,x} V_\beta + N_{\alpha,y} N_{\beta,y} V_\beta) dA - Ri \int_A N_\alpha N_\beta \theta_\beta dA + \\ & \frac{Ha^2}{Re} \int_A N_\alpha N_\beta V_\beta dA = \int_{S_0} N_\alpha S_y dS_0 \end{aligned} \quad (3.25)$$

$$\begin{aligned} & \int_A N_\alpha \left[(N_\beta U_\beta)(N_{\gamma,x} \theta_\gamma) + (N_\beta V_\beta)(N_{\gamma,y} \theta_\gamma) \right] dA + \\ & \frac{1}{Re Pr} \int_A (N_{\alpha,x} N_{\beta,x} \theta_\beta + N_{\alpha,y} N_{\beta,y} \theta_\beta) dA = \int_{S_w} N_\alpha q_w dS_w \end{aligned} \quad (3.26)$$

Then the finite element equations can be written in the form

$$K_{\alpha\beta^x} U_\beta + K_{\alpha\beta^y} V_\beta = 0 \quad (3.27)$$

$$K_{\alpha\beta\gamma^x} U_\beta U_\gamma + K_{\alpha\beta\gamma^y} V_\beta U_\gamma + M_{\lambda\mu^x} P_\mu - \frac{1}{Re} (S_{\alpha\beta^{xx}} + S_{\alpha\beta^{yy}}) U_\beta = Q_{\alpha^u} \quad (3.28)$$

$$\begin{aligned} & K_{\alpha\beta\gamma^x} U_\beta V_\gamma + K_{\alpha\beta\gamma^y} V_\beta V_\gamma + M_{\alpha\mu^y} P_\mu - \frac{1}{Re} (S_{\alpha\beta^{xx}} + S_{\alpha\beta^{yy}}) V_\beta - Ri K_{\alpha\beta} \theta_\beta \\ & + \frac{Ha^2}{Re} K_{\alpha\beta} V_\beta = Q_{\alpha^v} \end{aligned} \quad (3.29)$$

$$K_{\alpha\beta\gamma^x} U_\beta \theta_\gamma + K_{\alpha\beta\gamma^y} V_\beta \theta_\gamma - \frac{1}{Re Pr} (S_{\alpha\beta^{xx}} + S_{\alpha\beta^{yy}}) \theta_\beta = Q_{\alpha^\theta} \quad (3.30)$$

where the coefficients in element matrices are in the form of the integrals over the element area and along the element edges S_0 and S_w as

$$K_{\alpha\beta^x} = \int_A N_\alpha N_{\beta,x} dA \quad (3.31a)$$

$$K_{\alpha\beta^y} = \int_A N_\alpha N_{\beta,y} dA \quad (3.31b)$$

$$K_{\alpha\beta\gamma^x} = \int_A N_\alpha N_\beta N_{\gamma,x} dA \quad (3.31c)$$

$$K_{\alpha\beta\gamma^y} = \int_A N_\alpha N_\beta N_{\gamma,y} dA \quad (3.31d)$$

$$K_{\alpha\beta} = \int_A N_\alpha N_\beta dA \quad (3.31e)$$

$$S_{\alpha\beta^{xx}} = \int_A N_{\alpha,x} N_{\beta,x} dA \quad (3.31f)$$

$$S_{\alpha\beta^{yy}} = \int_A N_{\alpha,y} N_{\beta,y} dA \quad (3.31g)$$

$$M_{\lambda\mu^x} = \int_A H_\lambda H_{\mu,x} dA \quad (3.31h)$$

$$M_{\alpha\mu^y} = \int_A H_\alpha H_{\mu,y} dA \quad (3.31i)$$

$$Q_{\alpha^u} = \int_{S_0} N_\alpha S_x dS_0 \quad (3.31j)$$

$$Q_{\alpha^v} = \int_{S_0} N_\alpha S_y dS_0 \quad (3.31k)$$

$$Q_{\alpha^\theta} = \int_{S_w} N_\alpha q_w dS_w \quad (3.31l)$$

These element matrices are evaluated in a closed form ready for numerical simulation. Details of the derivation for these element matrices are omitted herein. For numerical simulation, these element matrices are evaluated in closed-form. Details of the derivation for these element matrices are omitted herein for brevity.

The resultant finite element equations (3.27) - (3.30), are nonlinear. These nonlinear algebraic equations are solved employing the Newton-Raphson iteration technique by first writing the unbalanced values from the set of the finite element equations (3.27) - (3.30) as

$$F_{\alpha^p} = K_{\alpha\beta^x} U_\beta + K_{\alpha\beta^y} V_\beta \quad (3.32a)$$

$$F_{\alpha^u} = K_{\alpha\beta\gamma^x} U_\beta U_\gamma + K_{\alpha\beta\gamma^y} V_\gamma U_\gamma + M_{\alpha\mu^x} P_\mu - \frac{1}{Re} (S_{\alpha\beta^{xx}} + S_{\alpha\beta^{yy}}) U_\beta - Q_{\alpha^u} \quad (3.32b)$$

$$F_{\alpha^v} = K_{\alpha\beta\gamma^x} U_\beta V_\gamma + K_{\alpha\beta\gamma^y} V_\gamma V_\gamma + M_{\alpha\mu^y} P_\mu - \frac{1}{Re} (S_{\alpha\beta^{xx}} + S_{\alpha\beta^{yy}}) V_\beta - Ri K_{\alpha\beta} \theta_\beta + \frac{Ha^2}{Re} K_{\alpha\beta} V_\beta - Q_{\alpha^v} \quad (3.32c)$$

$$F_{\alpha^\theta} = K_{\alpha\beta\gamma^x} U_\beta \theta_\gamma + K_{\alpha\beta\gamma^y} V_\beta \theta_\gamma - \frac{1}{Re Pr} (S_{\alpha\beta^{xx}} + S_{\alpha\beta^{yy}}) \theta_\beta - Q_{\alpha^\theta} \quad (3.32d)$$

This leads to a set of algebraic equations with the incremental unknowns of the element nodal velocity components, temperatures, and pressures in the form,

$$\begin{bmatrix} K_{uu} & K_{uv} & K_{u\theta} & K_{up} \\ K_{vu} & K_{vv} & K_{v\theta} & K_{vp} \\ K_{\theta u} & K_{\theta v} & K_{\theta\theta} & 0 \\ K_{pu} & K_{pv} & 0 & 0 \end{bmatrix} \begin{bmatrix} \Delta u \\ \Delta v \\ \Delta \theta \\ \Delta p \end{bmatrix} = \begin{bmatrix} F_{\alpha^u} \\ F_{\alpha^v} \\ F_{\alpha^\theta} \\ F_{\alpha^p} \end{bmatrix} \quad (3.33)$$

$$\text{where, } K_{uu} = K_{\alpha\beta\gamma^x} U_\beta + K_{\alpha\beta\gamma^x} U_\gamma + K_{\alpha\beta\gamma^y} V_\beta - \frac{1}{Re} (S_{\alpha\beta^{xx}} + S_{\alpha\beta^{yy}})$$

$$K_{uv} = K_{\alpha\beta\gamma^y} U_\gamma$$

$$K_{u\theta} = 0$$

$$K_{up} = M_{\alpha\mu^x}$$

$$K_{vu} = K_{\alpha\beta\gamma^x} V_\gamma$$

$$K_{vv} = K_{\alpha\beta\gamma^x} U_\beta + K_{\alpha\beta\gamma^y} V_\gamma + K_{\alpha\beta\gamma^y} V_\gamma - \frac{1}{Re} (S_{\alpha\beta^{xx}} + S_{\alpha\beta^{yy}})$$

$$K_{v\theta} = - Ri K_{\alpha\beta}$$

$$K_{vp} = M_{\alpha\mu^y}$$

$$K_{\theta u} = K_{\alpha\beta\gamma^x} \theta_\gamma$$

$$K_{\theta v} = K_{\alpha\beta\gamma^y} \theta \gamma$$

$$K_{\theta\theta} = K_{\alpha\beta\gamma^x} U_\beta + K_{\alpha\beta\gamma^y} V_\beta - \frac{1}{Re Pr} (S_{\alpha\beta^{xx}} + S_{\alpha\beta^{yy}})$$

$$K_{pu} = M_{\alpha\mu^x}$$

$$K_{pv} = M_{\alpha\mu^y} \text{ and } K_{\theta p} = K_{p\theta} = K_{pp} = 0$$

The iteration process is terminated if the percentage of the overall change compared to the previous iteration is less than the specified value.

To solve the sets of the global nonlinear algebraic equations in the form of a matrix, the Newton-Raphson iteration technique has been adapted through PDE solver with MATLAB interface. The convergence of solutions is assumed when the relative error for each variable between consecutive iterations is recorded below the convergence criterion ε such that,

$|\Psi^{n+1} - \Psi^n| < \varepsilon$, where n is a number of iteration and $\Psi = U, V, \theta$. The convergence criterion was set to 10^{-5} .

3.3.2 Grid Size Sensitivity Test

In order to determine a proper grid size for the present study at $Pr = 0.71$, $Ri = 1$, $A = 0.1$, $\lambda = 2$, $L = 0.45$ and $D = 0.50$, a grid independent test was analyzed with five types of meshes, average Nusselt number of the fin surface is obtained. This is described in Table 3.1 and as seen in Figure 3.2

Table 3.1: Grid sensitivity check at $Pr = 0.71$, $Ri = 1$, $\lambda = 2$, $L = 0.45$ and $D = 0.50$

Nodes	931	1213	1823	6844	25133
Elements	1700	2245	3421	13273	49464
Nu_{av}	5.1290	5.2303	5.3952	5.6491	5.6574
Time (s)	7	10	13	21	38

Table 3.1 is presented the average Nusselt number of the fin surface for different grids. As it can be observed from the table, the grid size of 6844 nodes and 13273 elements provided a satisfactory solution for the present numerical investigation.

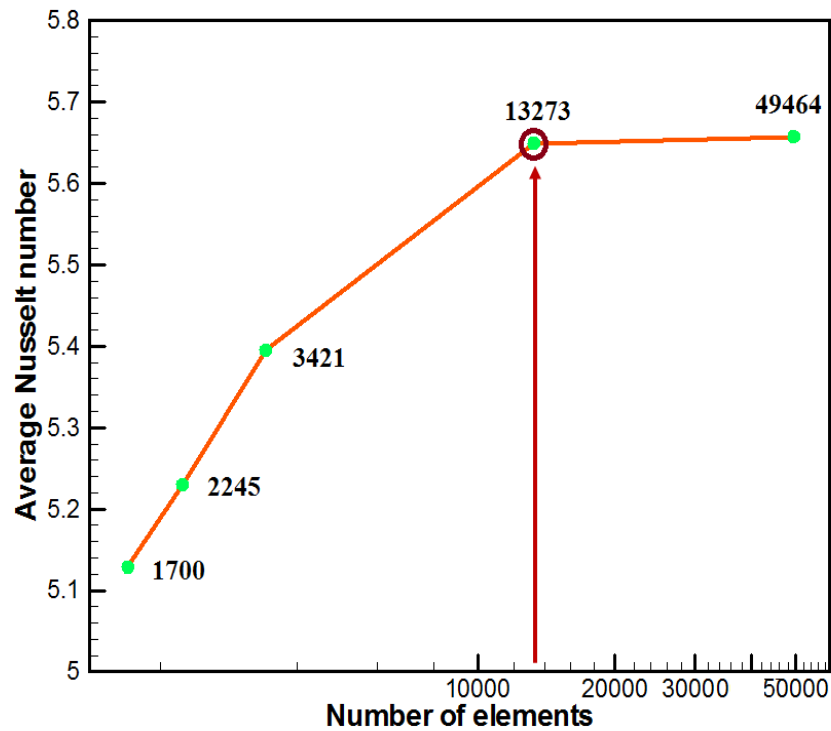


Figure 3.2: Grid independency study for different elements while $Pr = 0.71$, $Ri = 1$, $Ha = 10$, $A = 0.1$, $\lambda = 2$, $L = 0.45$ and $D = 0.50$

3.3.3 Validation of the Numerical Scheme

In order to check the accuracy of the numerical results obtained in this problem, the average Nusselt number along the right cold wall was compared with the results presented by Nag et al. [27] and Elatar et al. [39] at $L = 0.20$ and $Ra = 10^6$.

Table 3.2: Comparison of average Nusselt number on cold wall for $L = 0.20$, $Pr = 0.71$ and $Ra = 10^6$

B	0.02	0.04	0.1
Nag et al. [27]	8.861	8.888	9.033
Elatar et al. [39]	8.672	8.710	8.947
Present results	8.783	8.838	8.985

The average Nusselt number values as seen in Table 3.2 shows good agreement. In addition, a comparison of the streamlines and isotherms is made for the present results with those of Tasnim and Collins [31] and Elatar et al. [39] at $Ra = 10^5$, $B = 0.01$, $L = 0.5$ and $D = 0.75$) as shown in Figure 3.3. The shapes of streamline contours are almost identical. For the isotherms, one can see the strong agreement of the present results with those by Tasnim and Collins [31] and Elatar et al. [39] as seen in Figure 3.3

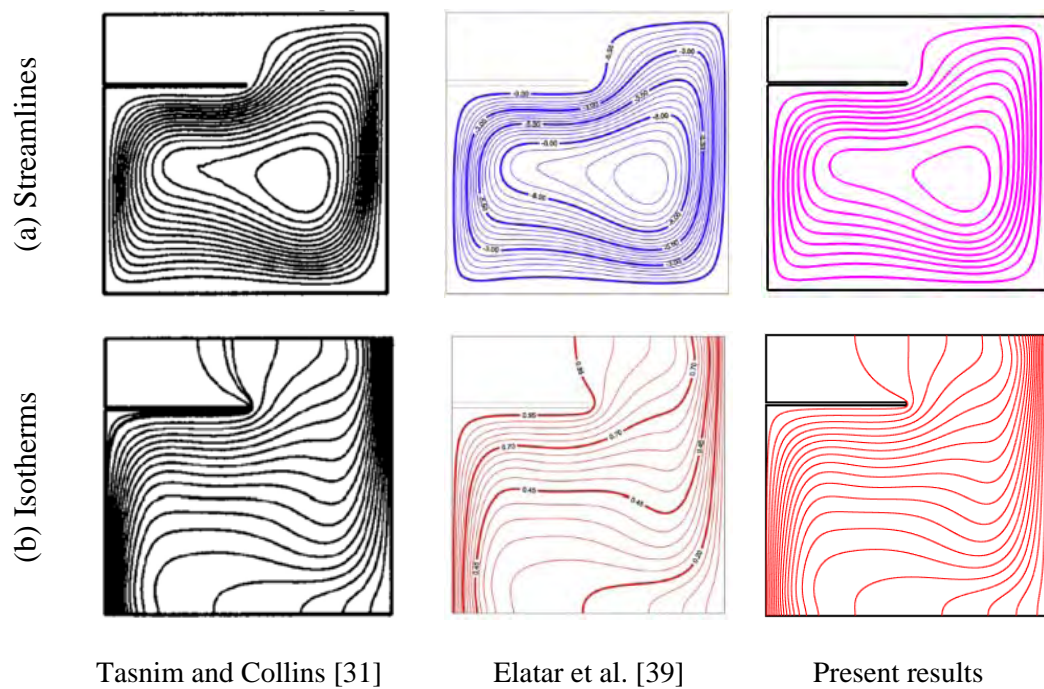


Figure 3.3: Comparison of Streamlines and isotherms with $Pr = 0.71$, $Ra = 10^5$, $B = 0.1$, $L = 0.50$ and $D = 0.75$

CHAPTER 4

RESULTS AND DISCUSSION

A numerical study has been performed through the finite element method to analyze the laminar mixed convection heat transfer and fluid flow in a lid-driven wavy cavity having vertical fin. Numerical results are presented in order to determine the effects of the considered parameters. The dimensionless parameters specified for the system are Richardson number (Ri), Hartmann number (Ha) and physical parameter for the fin length (L) of the wavy cavity. Results are presented through streamline and isotherms along with necessary plots at the three different fin length $L = 0.25, 0.35$ and 0.45 along with fin thickness $B = 0.04$, fin position $D = 0.50$, amplitude $A = 0.1$ of oscillations $\lambda = 2$, $Re = 100$ and Prandtl number $Pr = 0.71$ for different values of $Ri = 0.1$ to 10 , and $Ha = 0$ to 60 . Furthermore, the velocity profiles, local Nusselt number, and heat transfer rate in terms of the average Nusselt number (Nu_{av}) and the average fluid temperature (θ_{av}) are displayed. Finally, the performance of fin expressed in terms of the fin effectiveness (ϵ_f) is also displayed.

4.1 CASE 1 (Effect of Fin Length When $L = 0.25$)

In this section, results of the numerical investigation of mixed convection heat transfer in presence of magnetic field in a lid-driven wavy cavity having vertical fin are numerically presented. The results have been obtained fin length 0.25 for the Richardson number, Hartmann number and the rate of heat transfer. The results of this parametric study are shown in Figure 4.1- 4.8.

4.1.1 Effect of Richardson number

The effects of Richardson number Ri ($= 0.1, 1, 5, 10$) on streamlines and isotherms for the present configuration at $Ha = 10$, $Pr = 0.71$, $L = 0.25$, $A = 0.1$ and $\lambda = 2$ has been demonstrated in Figure 4.1(a)–(b) in terms of dimensionless velocity profiles along the horizontal centre line and local Nusselt number along the bottom hot wall are shown in Figure 4.2 and Figure 4.3 respectively. Richardson number represents the relative importance of mixed convection or combined forced convection and free convection. From Figure 4.1 (a), it is seen that when $Ri = 0.1$ the strength of

buoyancy force inside the cavity is significant and one vortex appear inside the cavity generated by the movement of the lid wall.

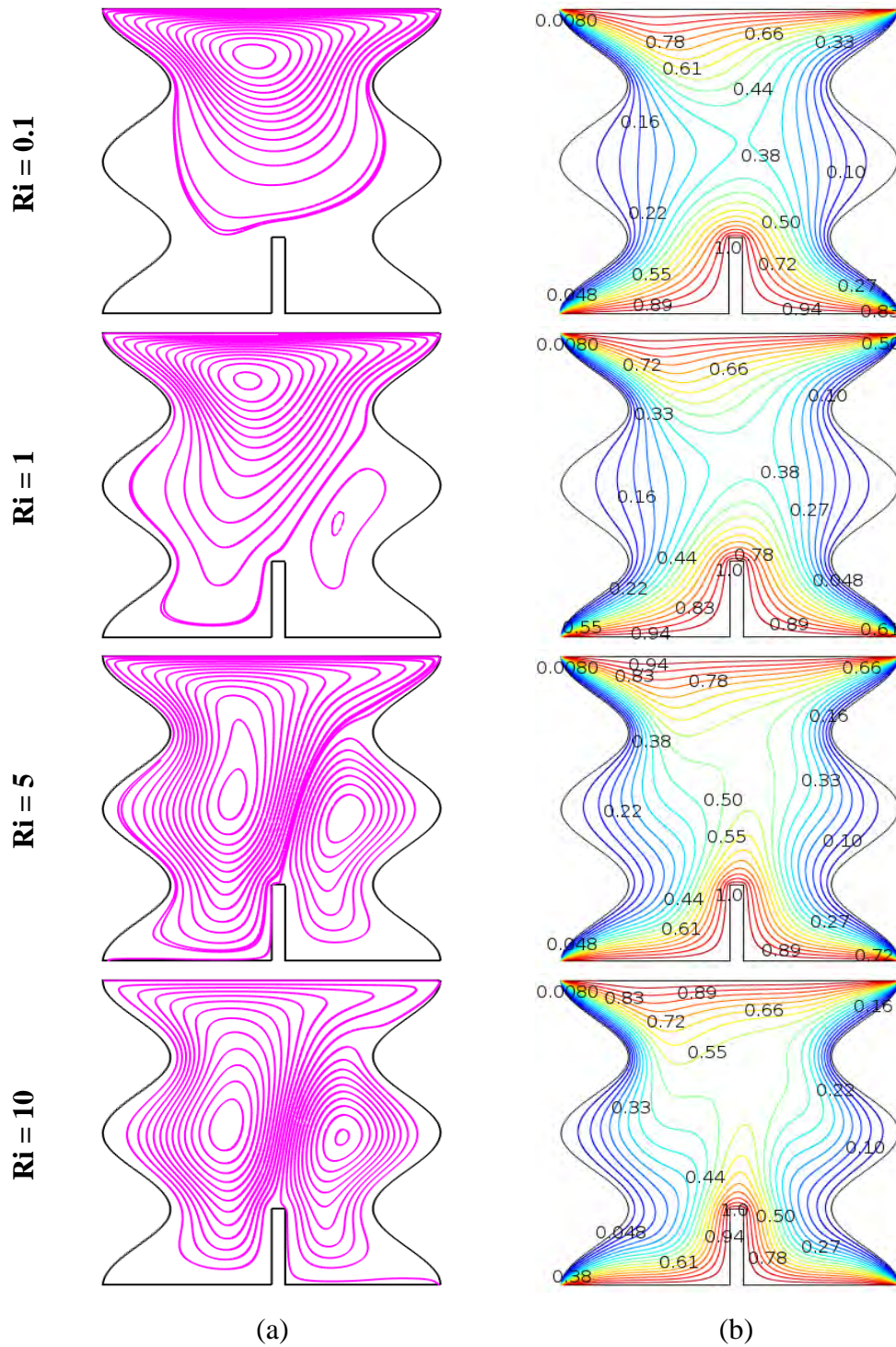


Figure 4.1: Effect of Richardson number on (a) streamlines and (b) isotherms for $L = 0.25$, $Pr = 0.71$, $Ha = 10$ and $\lambda = 2$

Again when $Ri = 1$ the flow structure is similar to $Ri = 0.1$ but two vortices appear inside the cavity which one is major vortex and another one is a minor vortex. Further again when Richardson number increases ($Ri = 5$ and 10), the strength of the buoyancy force is more significant and two vortices appear to move down the right half and left half of the cavity. The physical fact behind it's that the greater effect of the Richardson number increases the buoyancy force to influence the flow field. Conduction dominant heat transfer is observed from the isotherms in Figure 4.1 (b) at $L = 0.25$ and $Ha = 10$, it is clear that the thick thermal boundary layer exists near to the heated walls (top and bottom walls) and the fin surface due to the lower value of $Ri = 0.1$ and these become thinner with higher value of $Ri = 10$. The curvature of the isotherms increases with increasing Ri and the heat lines are condensed to the vertical wavy walls and the fin surface, which means increasing heat transfer through convection.

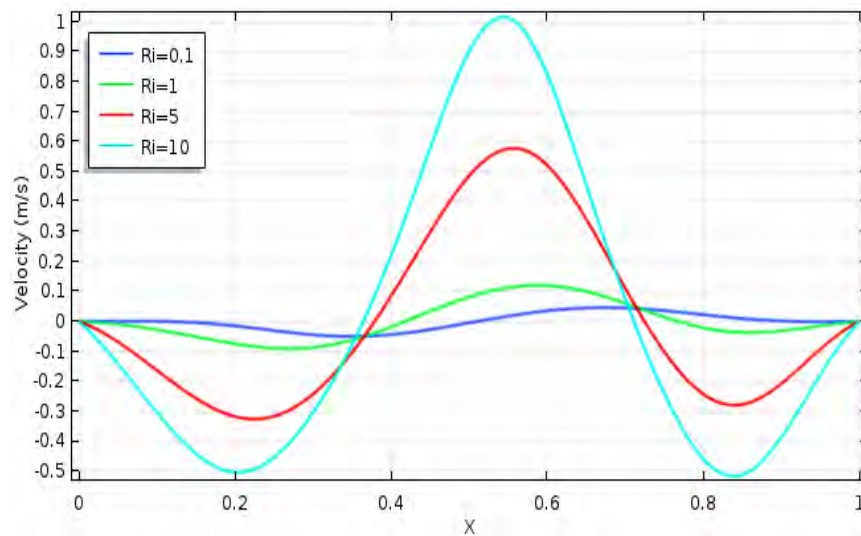


Figure 4.2: Variation of velocity profiles along the horizontal centre line of cavity for $L = 0.25$, $B = 0.04$, $D = 0.50$, $Ha = 10$ and $Pr = 0.71$ varying Ri

The effect of Richardson number (Ri) on the vertical component of the velocity profiles along the horizontal centre line of the cavity at $L = 0.25$ and $Ha = 10$ is displayed in Figure 4.2. It can be seen from the figure that for lower values of Richardson number, velocity profiles bring smaller change but the higher value of Richardson number, velocity profiles causes larger change. Moreover, the absolute

value of the maximum and minimum value of the velocity increases with increasing Richardson number (increasing the buoyancy force).

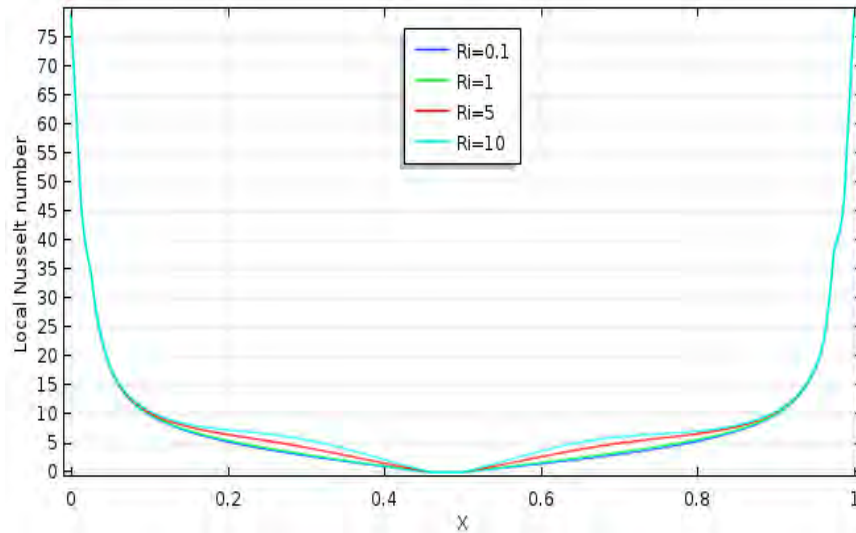


Figure 4.3: Variation of local Nusselt number along the bottom heated wall of cavity for $L = 0.25$, $B = 0.04$, $D = 0.50$, $Ha = 10$ and $Pr = 0.71$ varying Ri

The variation of the local Nusselt number distribution along the bottom heated wall of the enclosure for $D = 0.50$, $Pr = 0.71$, $L = 0.25$ and $Ha = 10$ varying Richardson number (Ri) is shown in Figure 4.3. It can be seen from the figure that the local Nusselt number increases with increasing Richardson number in a major portion of the bottom heated wall. It is also observed that the middle of the bottom wall (fin tip position $D = 0.50$ and thickness $B = 0.04$) the local Nusselt number is zero and does not change significantly with the increase in the Richardson number.

4.1.2 Effects of Hartmann number

The influence of Hartmann number on the streamlines and isotherms for different values of Ha ($= 0.0, 20.0, 40.0, 60.0$) with $Ri = 1.0$, $Pr = 0.71$, $L = 0.25$, $A = 0.1$ and $\lambda = 2$ has been demonstrated in Figure 4.4 (a)–(b) in terms of dimensionless velocity profiles and local Nusselt number along the horizontal centre line of the cavity are shown in Figure 4.5 and Figure 4.6 respectively. From Figure 4.4 (a) it can be seen that when $Ha = 0$ the strength of buoyancy force inside the cavity is more significant and two vortices appear inside the cavity which one is major vortex is produced by

the movement of the lid wall and another one is minor vortex produced by the right half of the cavity. Again when $Ha = 20$ and 40 the strength of buoyancy force inside the cavity is significant and two vortices appear inside the cavity.

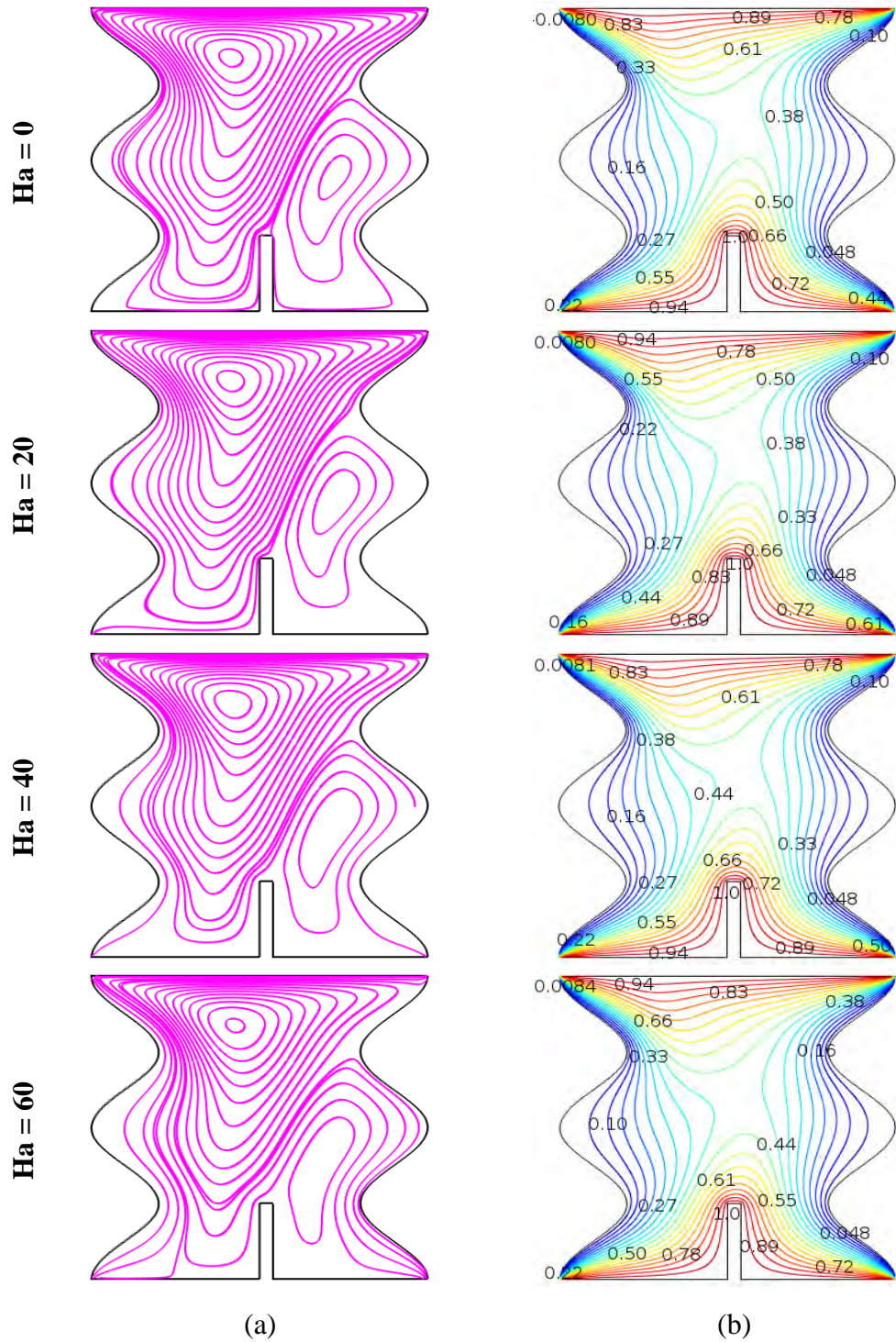


Figure 4.4: Effect of Hartmann number on (a) streamlines and (b) isotherms for $L = 0.25$, $Pr = 0.71$, $Ri = 1$ and $\lambda = 2$

Further again when $Ha = 60$, produced one vortex appear inside the cavity generated by the movement of the lid wall. The physical fact behind it's that the flow circulation decreases with increasing Hartmann number (increasing the strength of the magnetic field). This is because; applied magnetic field tends to slow down the fluid motions within the cavity. This means that the flow field strongly depends on the effect magnetic field. On the other hand, conduction dominant heat transfer is observed from the isotherms are almost similar and uniformly distributed due to the greater values of Hartmann number (Ha) is shown in Figure 4.4 (b); which is consistent to the effect of the magnetic field.

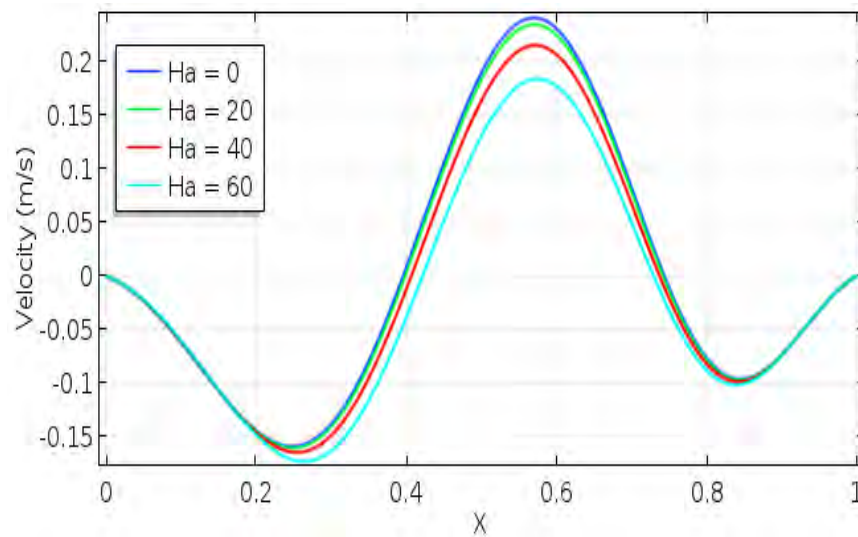


Figure 4.5: Variation of velocity profiles along the horizontal centre line of cavity for $L = 0.25$, $B = 0.04$, $D = 0.50$, $Ri = 1$ and $Pr = 0.71$ varying Ha

The effect of Hartmann number (Ha) on the vertical component of the velocity profiles along the horizontal centre line of the cavity at $L = 0.25$ and $Ri = 1$ is displayed in Figure 4.5. It can be observed that the changing rate of velocity is similar for every Hartmann number but different from each other. Moreover, the absolute value of the maximum and minimum value of the velocity increases with decreasing Hartmann number (increasing the buoyancy force).

The variation of the local Nusselt number distribution along the horizontal centre line of the enclosure for $D = 0.50$, $Pr = 0.71$, $L = 0.25$ and $Ri = 1$ varying Hartmann number (Ha) is shown in Figure 4.6. It can be seen from the figure that the changing rate of local Nusselt number is similar for every Hartmann number but different from

each other. Moreover, the local Nusselt number has two concaves up and one concave down the effect for every Hartmann number.

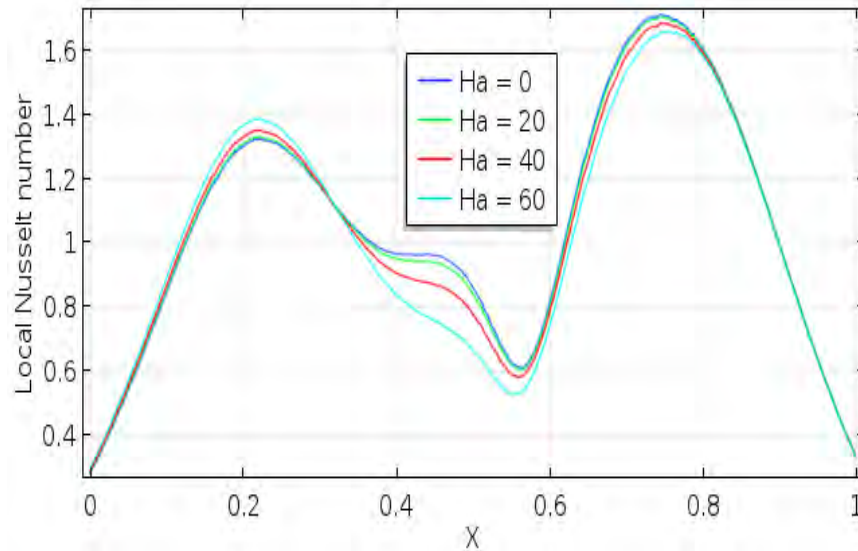


Figure 4.6: Variation of local Nusselt number along horizontal centre line of cavity for $L = 0.25$, $B = 0.04$, $D = 0.50$, $Ri = 1$ and $Pr = 0.71$ varying Ha

4.1.3 Heat Transfer Rates

In this section, results of the numerical investigation of mixed convection heat transfer in presence of magnetic field in a lid-driven wavy cavity having vertical fin are numerically presented. The average Nusselt number versus Hartmann numbers and Richardson numbers heat transfer rates are shown in Figure 4.7-4.8 and heat transfer rates Table 4.1-4.2 given below.

Table 4.1: Numerical values of average Nusselt number against Ha on the right cold wall for selected value Ri while $Pr = 0.71$, $L = 0.25$, $B = 0.04$ and $D = 0.50$

Ha	Average Nusselt Number (Nu_{av})			
	$Ri = 0.1$	$Ri = 1$	$Ri = 5$	$Ri = 10$
0	6.3764	6.4095	6.6872	6.9981
20	6.3541	6.3794	6.6539	6.9670
40	6.3417	6.3637	6.6471	6.9684
60	6.3312	6.3561	6.6327	6.9602

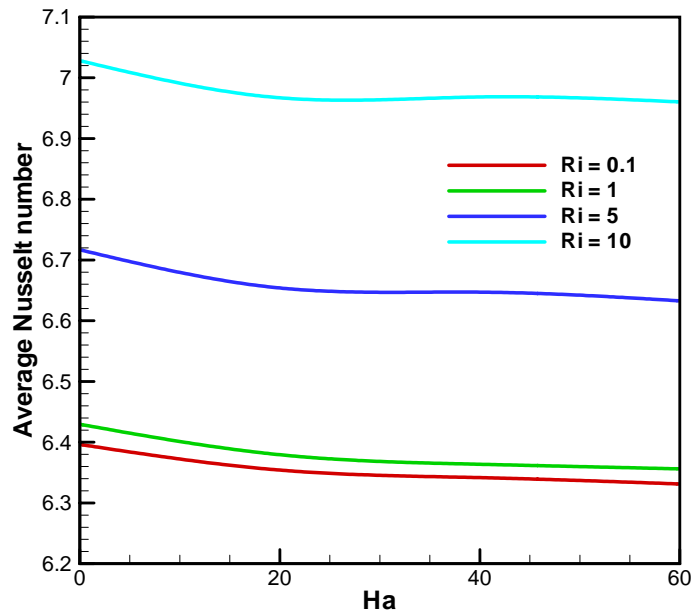


Figure 4.7: Variation of the average Nusselt number against Ha for selected value Ri while $Pr = 0.71$, $L = 0.25$, $B = 0.04$ and $D = 0.50$

Figure 4.7 illustrate that the average Nusselt number (Nu_{av}) versus Hartmann number along the right cold wall for various Richardson number (Ri) with fin length $L = 0.25$ and $Pr = 0.71$ while the value of the remaining parameters is kept fixed. It can be seen from this Figure, the average Nusselt number increases when the value of the Richardson number increases. At a constant Richardson number, with a decrease in Hartmann number the buoyancy force increases and the heat transfer is enhanced.

Table 4.2: Numerical values of average fluid temperature against Ri for selected value Ha while $Pr = 0.71$, $L = 0.25$, $B = 0.04$ and $D = 0.50$

Ri	Average Temperature (θ_{av})			
	$Ha = 0$	$Ha = 20$	$Ha = 40$	$Ha = 60$
0.1	0.44621	0.44362	0.44253	0.44227
1	0.45074	0.44907	0.44849	0.44837
5	0.47049	0.46671	0.46457	0.46388
10	0.47290	0.46795	0.46513	0.46423

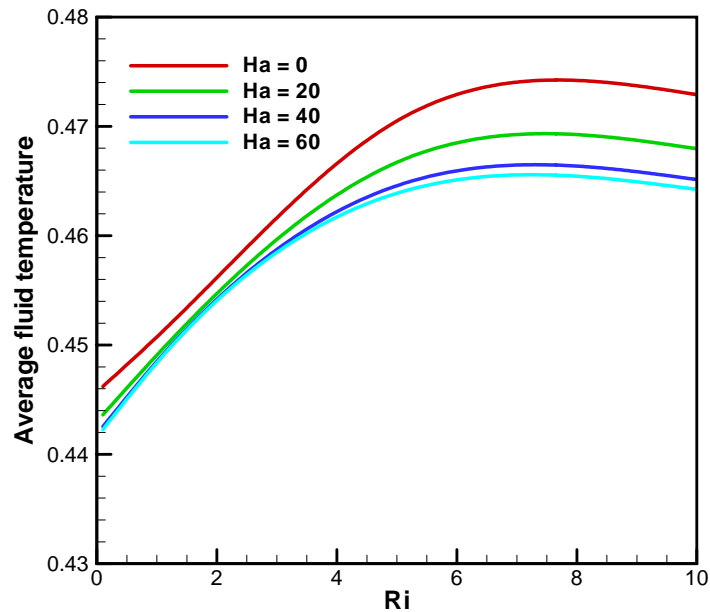


Figure 4.8: Variation of the average fluid temperature against Ri for selected value Ha while $Pr = 0.71$, $L = 0.25$, $B = 0.04$ and $D = 0.50$

Figure 4.8 illustrate that the average fluid temperature (θ_{av}) versus Richardson number (Ri) for various values of Hartmann number (Ha) with the fin length $L = 0.25$ and $Pr = 0.71$ while the value of the remaining parameters is kept constant. It can be seen from this figure, average fluid temperature increases when the value of Hartmann number decreases. It is also seen from this figure, average fluid temperature increases steadily with increasing Ri when Hartmann number is kept constant.

Table 4.1 - 4.2 represent the values of the average Nusselt number and average fluid temperature respectively for considered parameters including $L = 0.25$, Ri , Pr , Ha and B respectively. Both the numerical result indicates that the average Nusselt number and average fluid temperature increases with increasing the value of Ri and decrease with the higher value of Ha .

Finally, both heat transfer rate and average temperature increase with increasing of Richardson number for all values of Hartmann number. At a constant Hartmann

number, with an increase in Richardson number the buoyancy force increases and heat transfer is enhanced.

4.2 CASE 2 (Effect of Fin Length When $L = 0.35$)

In this section, results of the numerical investigation of mixed convection heat transfer in presence of magnetic field in a lid-driven wavy cavity having vertical fin are numerically presented. The results have been obtained fin length 0.35 for the Richardson number, Hartmann number and the rate of heat transfer. The results of this parametric study are shown in Figure 4.9- 4.16.

4.2.1 Effect of Richardson number

The effects of Richardson number Ri ($= 0.1, 1.0, 5.0, 10.0$) on streamlines and isotherms for the present configuration at $Ha = 10$, $Pr = 0.71$, $L = 0.35$, $A = 0.1$ and $\lambda = 2$ has been demonstrated in figure 4.9 (a)–(b) in terms of dimensionless velocity profiles along the horizontal centre line and local Nusselt number along the bottom hot wall are shown in Figure 4.10 and Figure 4.11 respectively. From Figure 4.9 (a), it is seen that when $Ri = 0.1$ the strength of buoyancy force inside the cavity is significant and one vortex appear inside the cavity generated by the movement of the lid wall. Again when $Ri = 1$ the flow structure is similar to $Ri = 0.1$ but two vortices appear inside the cavity which one is major vortex and another one is a minor vortex. Further again when Ri increases ($Ri = 5$ and 10), the strength of the buoyancy force is more significant and two vortices appear to move down the right half and left half of the cavity. The physical fact behind it's that the greater effect of the Richardson number increases the buoyancy force to influence the flow field.

Conduction dominant heat transfer is observed from the isotherms in Figure 4.9 (b) at $L = 0.35$ and $Ha = 10$, it is clear that the thick thermal boundary layer exists near to the heated walls and the fin surface due to the lower value of $Ri = 0.1$ and these become thinner with higher value of $Ri = 10$. The curvature of the isotherms increases with increasing the Richardson number (Ri) and the heat lines are condensed to the wavy walls and the fin surface, which means increasing heat transfer through convection.

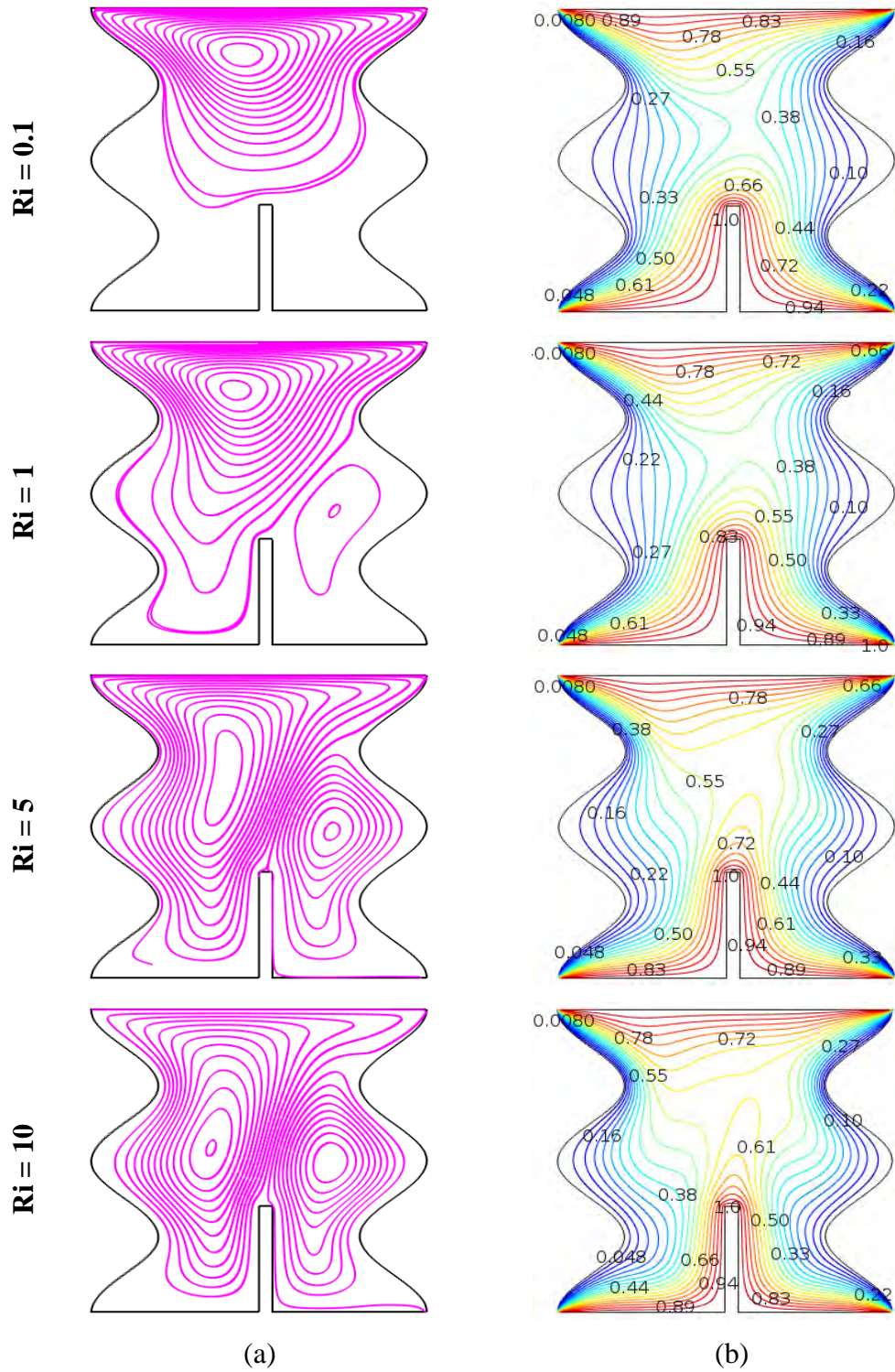


Figure 4.9: Effect of Richardson number on (a) streamlines and (b) isotherms for $L = 0.35$, $Pr = 0.71$, $Ha = 10$ and $\lambda = 2$

The effect of Richardson number (Ri) on the vertical component of the velocity profiles along the horizontal centre line of the cavity at $L = 0.35$ and $Ha = 10$ is displayed in Figure 4.10. It can be seen from the figure that for lower values of Richardson number, velocity profiles bring smaller change but the higher value of Richardson number, velocity profiles causes larger change. Moreover, the absolute value of the maximum and minimum value of the velocity increases with increasing Richardson number (Ri).

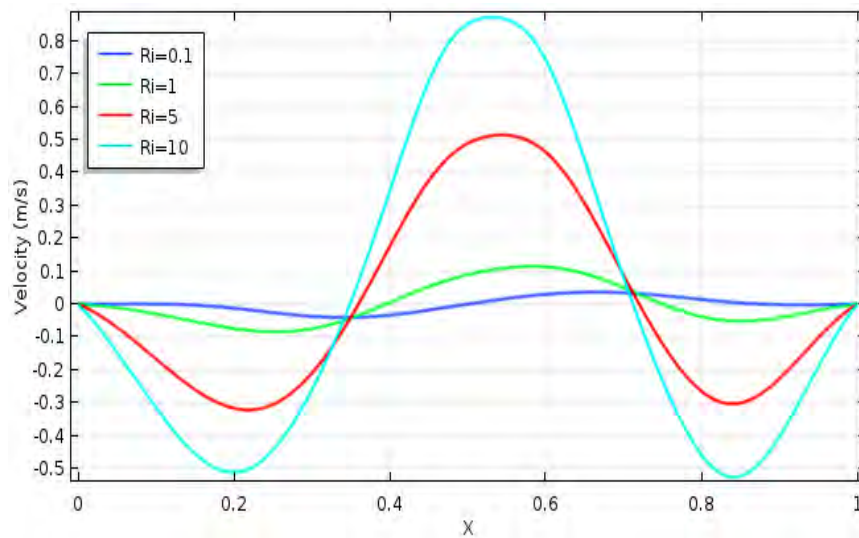


Figure 4.10: Variation of velocity profiles along the horizontal centre line of cavity with Richardson number for $L = 0.35$, at $Pr = 0.71$, $Ha = 10$ and $\lambda = 2$

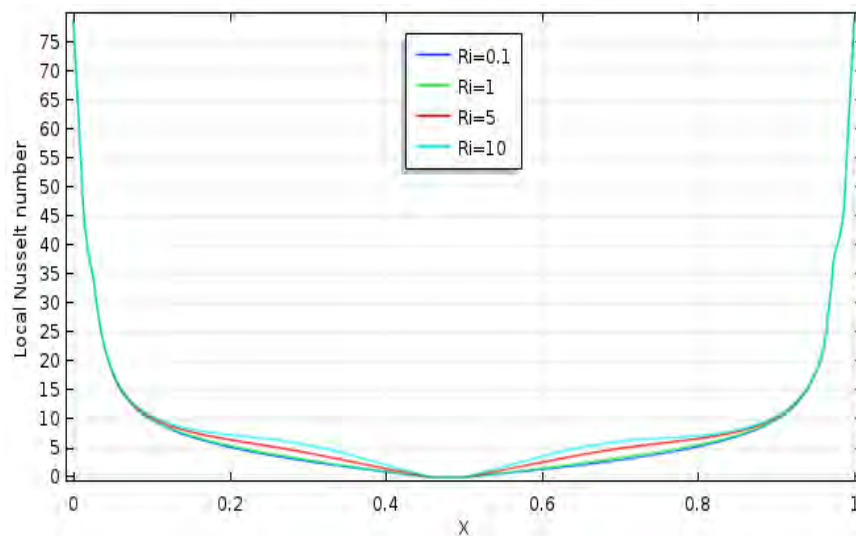


Figure 4.11: Variation of local Nusselt number along the bottom heated wall of cavity with Richardson number for $L = 0.35$ at $Pr = 0.71$, $Ha = 10$ and $\lambda = 2$

The variation of the local Nusselt number distribution along the bottom heated wall of the enclosure for $D = 0.50$, $Pr = 0.71$, $L = 0.35$ and $Ha = 10$ varying Richardson number (Ri) is shown in Figure 4.11. It can be seen from the figure that the local Nusselt number increases with increasing Richardson number in a major portion of the bottom heated wall. It is also observed that the middle of the bottom wall (fin tip position $D = 0.50$ and thickness $B = 0.04$) the local Nusselt number is zero and does not change significantly with the increase in the Richardson number.

4.2.2 Effects of Hartmann number

The influence of Hartman number on the streamlines and isotherms for different values of Ha ($= 0.0, 20.0, 40.0, 60.0$) with $Ri = 1.0$, $Pr = 0.71$, $L = 0.35$, $A = 0.1$ and $\lambda = 2$ has been demonstrated in figure 4.12 (a)–(b) in terms of dimensionless velocity profiles and local Nusselt number along the horizontal centre line of the cavity are shown in Figure 4.13 and Figure 4.14 respectively. From Figure 4.12 (a) it can be seen that when $Ha = 0$ the strength of buoyancy force inside the cavity is more significant and two vortices appear inside the cavity which one major vortex is produced by the movement of the lid wall and another one is minor vortex is produced by the right half of the cavity. Again when $Ha = 20$ and 40 the strength of buoyancy force inside the cavity is significant and two vortices appear inside the cavity. Further again when $Ha = 60$, produced are also two vortices appear inside the cavity. The physical fact behind it's that the flow circulation decreases with increasing Hartmann number (increasing the strength of the magnetic field). This is because; applied magnetic field tends to slow down the fluid motions within the cavity. This means that the flow field strongly depends on the effect of a magnetic field.

On the other hand, conduction dominant heat transfer is observed from the isotherms are almost similar for every Hartmann number and uniformly distributed due to the different values of Hartmann number (Ha) is shown in Figure 4.12 (b); which is consistent to the effect of the magnetic field.

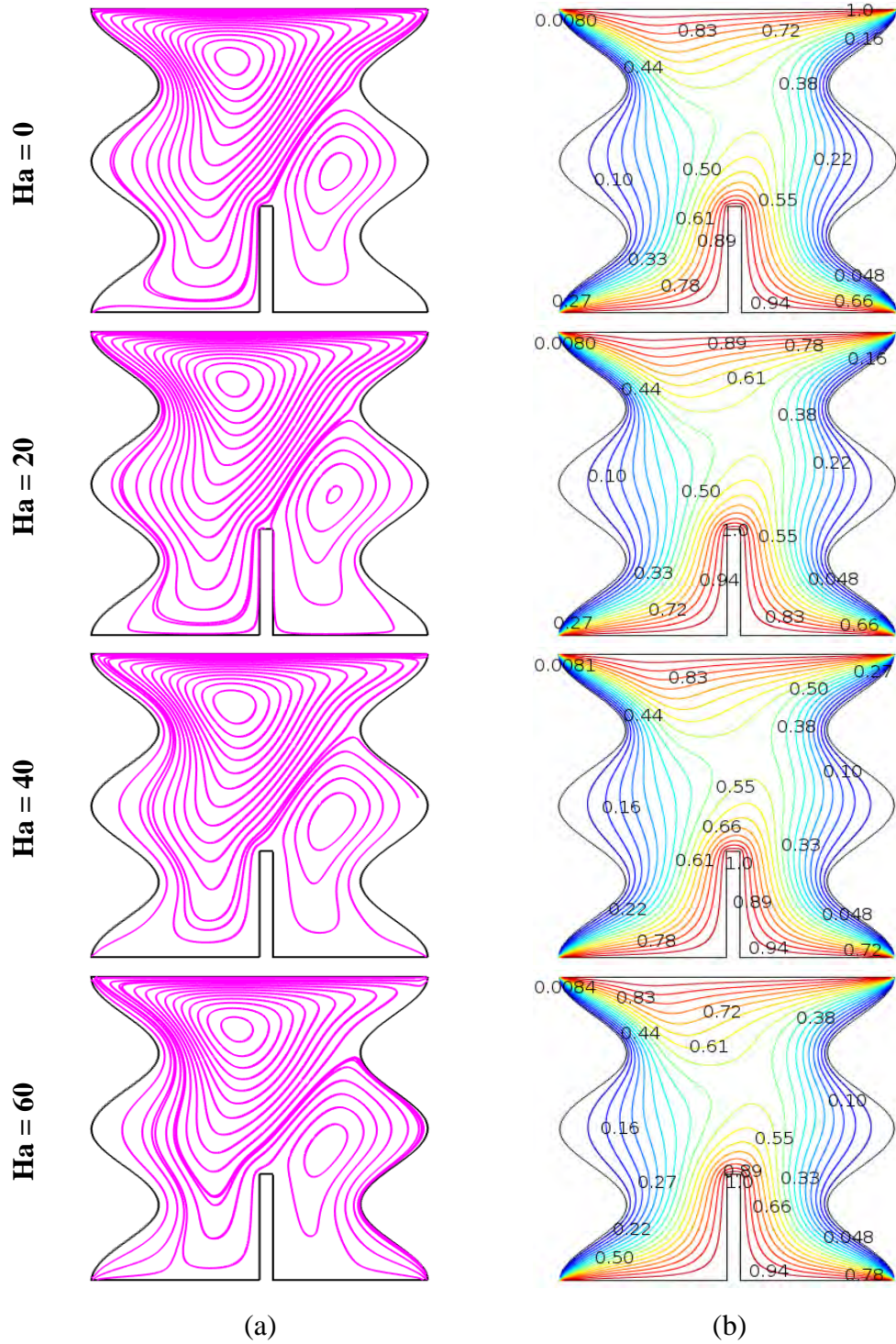


Figure 4.12: Effect of Hartmann number on (a) streamlines and (b) isotherms for $L = 0.35$, $Pr = 0.71$, $Ri = 1$ and $\lambda = 2$

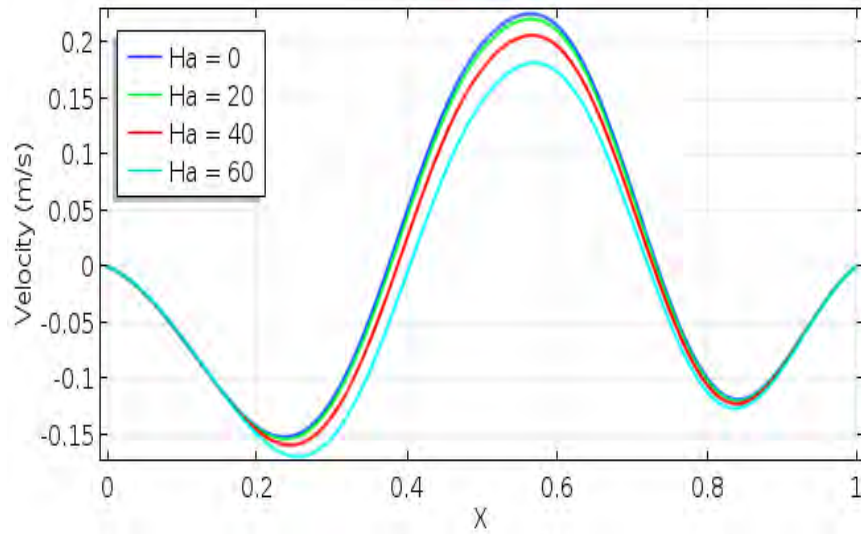


Figure 4.13: Variation of velocity profiles along the horizontal centre line of cavity for $L = 0.35$, $B = 0.04$, $D = 0.50$, $Ri = 1$ and $Pr = 0.71$ varying Ha

The effect of the Hartmann number (Ha) on the vertical component of the velocity profiles along the horizontal centre line of the cavity at $L = 0.35$ and $Ri = 1$ is displayed in Figure 4.13. It can be observed that the changing rate of velocity is almost similar for every Hartmann number but different from each other. Moreover, the absolute value of the maximum and minimum value of the velocity increases with decreasing Hartmann number (Ha).

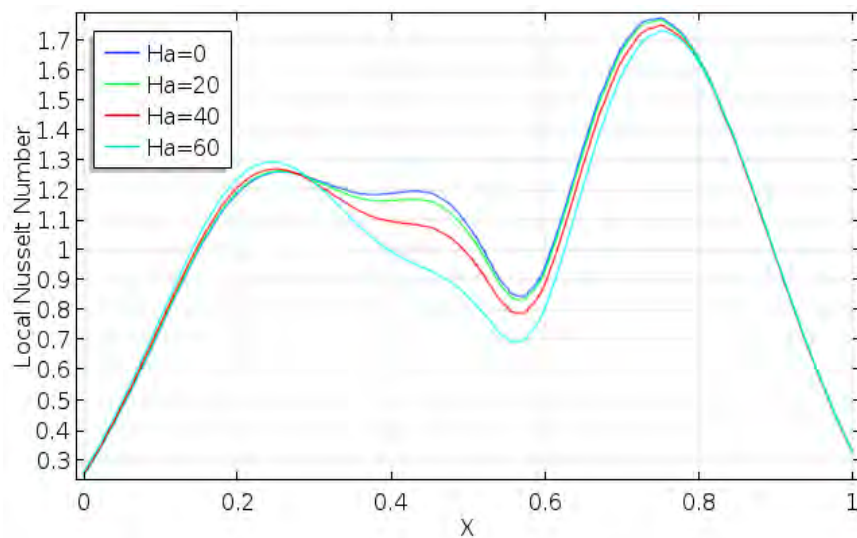


Figure 4.14: Variation of local Nusselt number along horizontal centre line of cavity for $L = 0.35$, $B = 0.04$, $D = 0.50$, $Ri = 1$ and $Pr = 0.71$ varying Ha

The variation of the local Nusselt number distribution along the horizontal centre line of the enclosure for $D = 0.50$, $Pr = 0.71$, $L = 0.35$ and $Ri = 1$ varying Hartmann number (Ha) is shown in Figure 4.14. It can be seen from the figure that the changing rate of local Nusselt number is similar for every Hartmann number but different from each other. Moreover, the local Nusselt number has two concaves up and one concave down the effect of Hartmann number.

4.2.3 Heat Transfer Rates

In this section, results of the numerical investigation of mixed convection heat transfer in presence of magnetic field in a lid-driven wavy cavity having vertical fin are numerically presented. The average Nusselt number versus Hartmann numbers and Richardson numbers heat transfer rates are shown in Figure 4.15-4.16 and heat transfer rates Table 4.3-4.4 given below.

Table 4.3: Numerical values of average Nusselt number against Ha on the right cold wall for selected value Ri while $Pr = 0.71$, $L = 0.35$, $B = 0.04$ and $D = 0.50$

Ha	Average Nusselt Number (Nu_{av})			
	$Ri = 0.1$	$Ri = 1$	$Ri = 5$	$Ri = 10$
0	6.5975	6.6529	6.9985	7.3648
20	6.5761	6.6137	6.9367	7.3077
40	6.5713	6.6105	6.9271	7.2946
60	6.5625	6.6027	6.9129	7.2841

Figure 4.15 illustrate the average Nusselt number (Nu_{av}) versus Hartmann number along the right cold wall for various Richardson number (Ri) with fin length $L = 0.35$ while the value of the remaining parameters is kept fixed. It can be seen from this figure, the average Nusselt number increases when the value of the Richardson number increases. At a constant Richardson number, with a decrease in Hartmann number the buoyancy force increases and the heat transfer are enhanced.

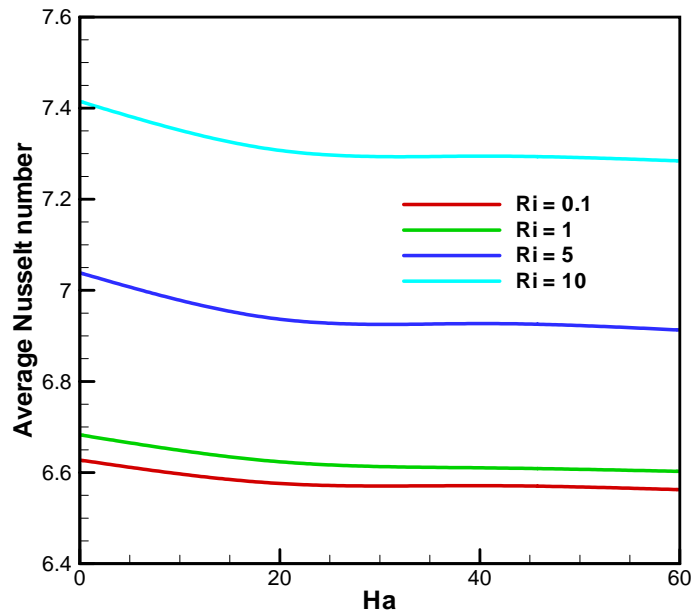


Figure 4.15: Variation of the average Nusselt number against Ha for selected value Ri while $Pr = 0.71$, $L = 0.35$, $B = 0.04$ and $D = 0.50$

Table 4.4: Numerical values of average fluid temperature against Ri for selected value Ha while $Pr = 0.71$, $L = 0.35$, $B = 0.04$ and $D = 0.50$

Ri	Average Temperature (θ_{av})			
	$Ha = 0$	$Ha = 20$	$Ha = 40$	$Ha = 60$
0.1	0.47661	0.47465	0.47373	0.47348
1	0.48250	0.48091	0.48014	0.47993
5	0.50282	0.49889	0.49654	0.49577
10	0.50690	0.50181	0.49879	0.49780

Figure 4.16 illustrate the average fluid temperature (θ_{av}) versus Richardson number (Ri) for various values of Hartmann number (Ha) with the fin length $L = 0.35$, while the value of the remaining parameters is kept constant. It can be seen from this figure, average fluid temperature increases when the value of Ha decreases. It is also seen from this figure, average fluid temperature increases steadily with increasing value of Richardson number when Hartmann number is kept constant.

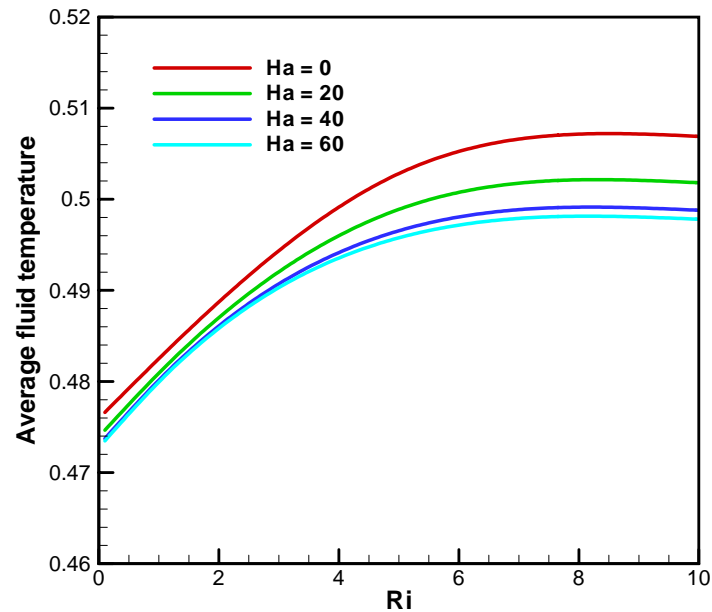


Figure 4.16: Variation of the average fluid temperature against Ri for selected value Ha while $Pr = 0.71$, $L = 0.35$, $B = 0.04$ and $D = 0.50$

Table 4.3 - 4.4 represent the values of the average Nusselt number and average fluid temperature respectively for considered parameters including Ri , Pr , Ha , $L = 0.35$ and B respectively. Both the numerical result indicates that the average Nusselt number and average fluid temperature increases with increasing the value of Ri and decrease with the higher value of Ha .

Finally, both heat transfer rate and average temperature increase with increasing of Richardson number for all values of Hartmann number. At a constant Hartmann number, with the increase in Richardson number the buoyancy force increases and heat transfer is enhanced.

4.3 CASE 3 (Effect of Fin Length When $L = 0.45$)

In this section, results of the numerical investigation of mixed convection heat transfer in presence of magnetic field in a lid-driven wavy cavity having vertical fin are numerically presented. The results have been obtained fin length 0.45 for the

Richardson number, Hartmann number and the rate of heat transfer. The results of this parametric study are shown in Figure 4.17- 4.24.

4.3.1 Effect of Richardson number

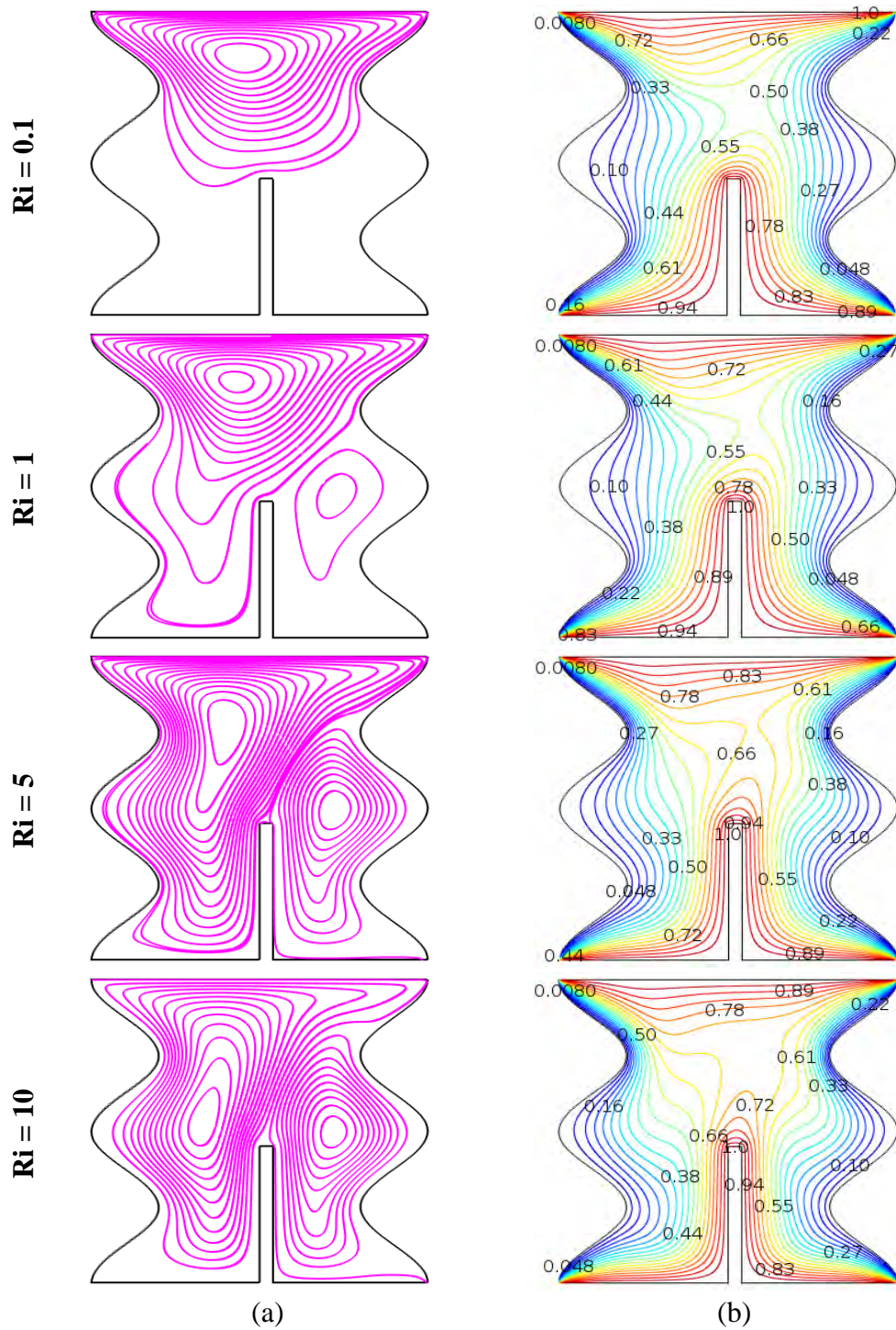


Figure 4.17: Effect of Richardson number on (a) streamlines and (b) isotherms for $L = 0.45$, $Pr = 0.71$, $Ha = 10$ and $\lambda = 2$

The effects of Richardson number Ri ($= 0.1, 1.0, 5.0, 10.0$) on streamlines and isotherms for the present configuration at $Ha = 10$, $Pr = 0.71$, $L = 0.45$, $A = 0.1$ and $\lambda = 2$ has been demonstrated in Figure 4.17 (a)–(b) in terms of velocity profiles along the horizontal centre line and local Nusselt number along the bottom hot wall are shown in Figure 4.18 and Figure 4.19 respectively. From Figure 4.17 (a), it is seen that when $Ri = 0.1$ the strength of buoyancy force inside the cavity is significant and one vortex appear inside the cavity generated by the movement of the lid wall. Again when $Ri = 1$ the flow structure is similar to $Ri = 0.1$ but two vortices appear inside the cavity which one is major vortex and another one is a minor vortex. Further again when Richardson number increases ($Ri = 5$ and 10), the strength of the buoyancy force is more significant and two vortices appear to move down the right half and left half of the cavity. The physical fact behind it's that the greater effect of the Richardson number increases the buoyancy force to influence the flow field. Conduction dominant heat transfer is observed from the isotherms in Figure 4.17 (b) at $L = 0.45$ and $Ha = 10$, it is clear that the thick thermal boundary layer exists near to the heated walls and the fin surface due to the lower value of $Ri = 0.1$ and these become thinner with higher value of $Ri = 10$. The curvature of the isotherms increases with increasing Ri and the heat lines are condensed to the wavy walls and the fin surface, which means increasing heat transfer through convection.

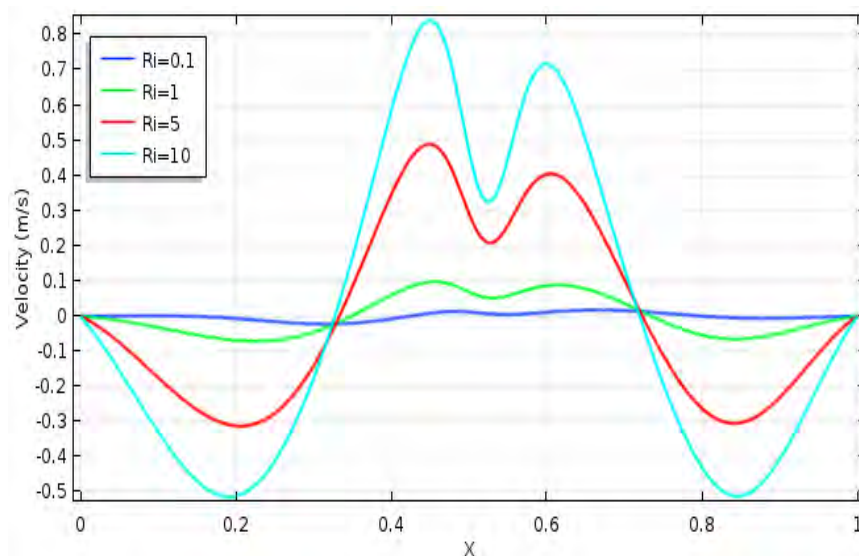


Figure 4.18: Variation of velocity profiles along the horizontal centre line of cavity with Richardson number for $L = 0.45$, at $Pr = 0.71$, $Ha = 10$ and $\lambda = 2$

The effect of Richardson number on the vertical component of the velocity profiles along the horizontal centre line of the cavity at $L = 0.45$, $\lambda = 2$, $Pr = 0.71$ and $Ha = 10$ is displayed in Figure 4.18. It can be seen from the figure that for lower values of Richardson number, velocity profiles bring smaller change but the higher value of Richardson number, velocity profiles causes higher change. Moreover, the absolute value of the maximum and minimum value of the velocity increases with increasing Richardson number (Ri).

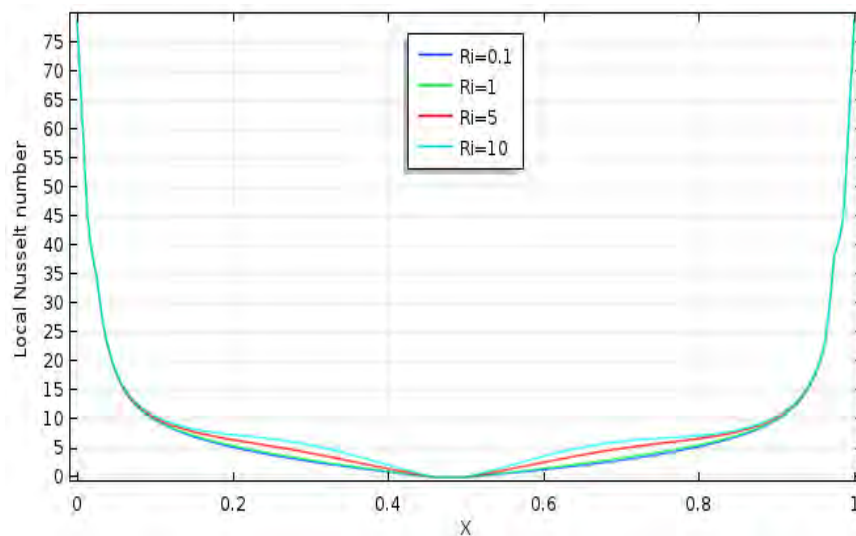


Figure 4.19: Variation of local Nusselt number along the bottom heated wall of cavity with Richardson number for $L = 0.45$ at $Pr = 0.71$, $Ha = 10$ and $\lambda = 2$

The variation of the local Nusselt number distribution along the bottom heated wall of the enclosure for $D = 0.50$, $Pr = 0.71$, $L = 0.45$ and $Ha = 10$ varying Richardson number (Ri) is shown in Fig. 4.19. It can be seen from the figure that the local Nusselt number increases with increasing Richardson number in a major portion of the bottom heated wall. It is also observed that the middle of the bottom wall (fin tip position $D = 0.50$ and thickness $B = 0.04$) the local Nusselt number is zero and does not change significantly with the increase in the Richardson number.

4.3.2 Effect of Hartmann number

The influence of Hartman number on the streamlines and isotherms for different values of Ha ($= 0.0, 20.0, 40.0, 60.0$) with $Ri = 1.0$, $Pr = 0.71$, $L = 0.25$, $A = 0.1$ and $\lambda = 2$ has been demonstrated in Figure 4.20 (a)–(b) in terms of dimensionless

velocity profiles and local Nusselt number along the horizontal centre line of the cavity are shown in Figure 4.21 and Figure 4.22 respectively.

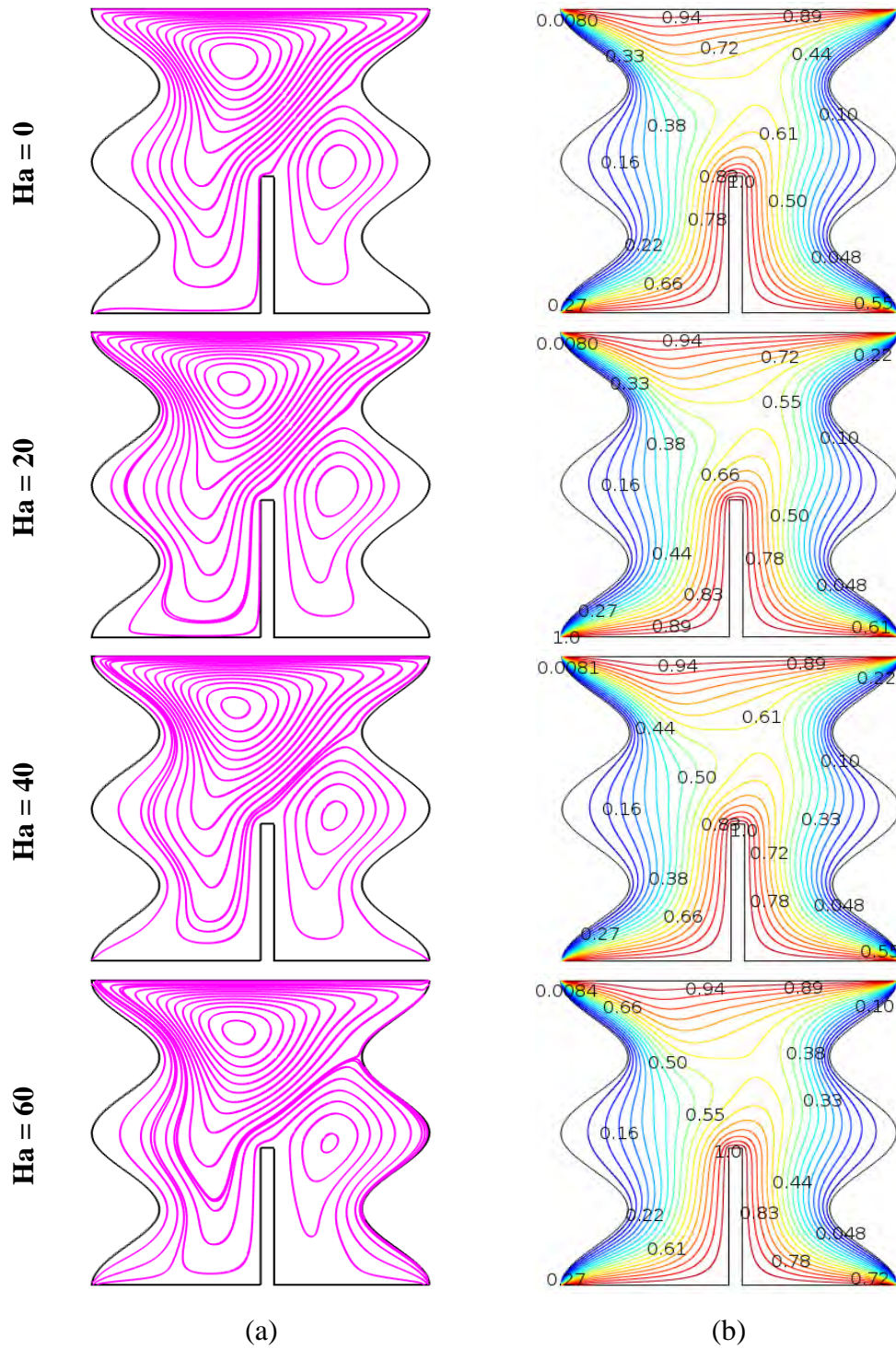


Figure 4.20: Effect of Hartmann number on (a) streamlines and (b) isotherms for $L = 0.45$, $Pr = 0.71$, $Ri = 1$ and $\lambda = 2$

From figure 4.20 (a) it can be seen that when $Ha = 0$ the strength of buoyancy force inside the cavity is more significant and two vortices appear inside the cavity which one major vortex is produced by the movement of the lid wall and another one is minor vortex is produced by the right half of the cavity. Again when $Ha = 20, 40$ and 60 the strength of buoyancy force inside the cavity is significant and also two vortices appear inside the cavity which one major vortex is produced by the movement of the lid wall and another one is minor vortex is produced by the right half of the cavity but the vorticity decreases with increasing Hartmann number. The physical fact behind it's that the flow circulation decreases with increasing Hartmann number. This is because; applied magnetic field tends to slow down the fluid motions within the cavity. This means that the flow field strongly depends on the effect magnetic field. On the other hand, conduction dominant heat transfer is observed from the isotherms are almost similar for every Hartmann and uniformly distributed due to the different values of Hartmann number (Ha) is shown in Figure 4.20 (b); which is consistent to the effect of the magnetic field.

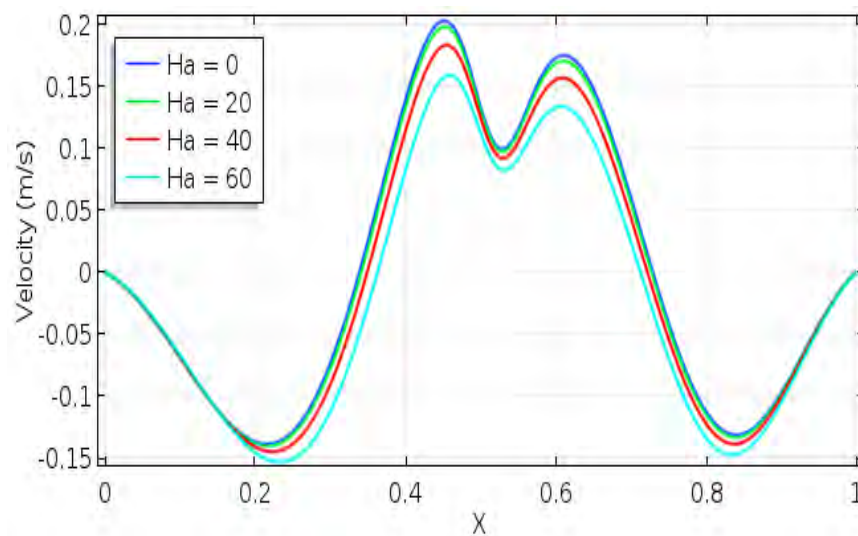


Figure 4.21: Variation of velocity profiles along the horizontal centre line of cavity for $L = 0.45$, $B = 0.04$, $D = 0.50$, $Ri = 1$ and $Pr = 0.71$ varying Ha

The effect of Hartmann number (Ha) on the vertical component of the velocity profiles along the horizontal centre line of the cavity at $L = 0.45$ and $Ri = 1$ is displayed in Figure 4.21. It can be observed that the changing rate of velocity is similar for every Hartmann number but different from each other. Moreover, the

absolute value of the maximum and minimum value of the velocity increases with decreasing Hartmann number.

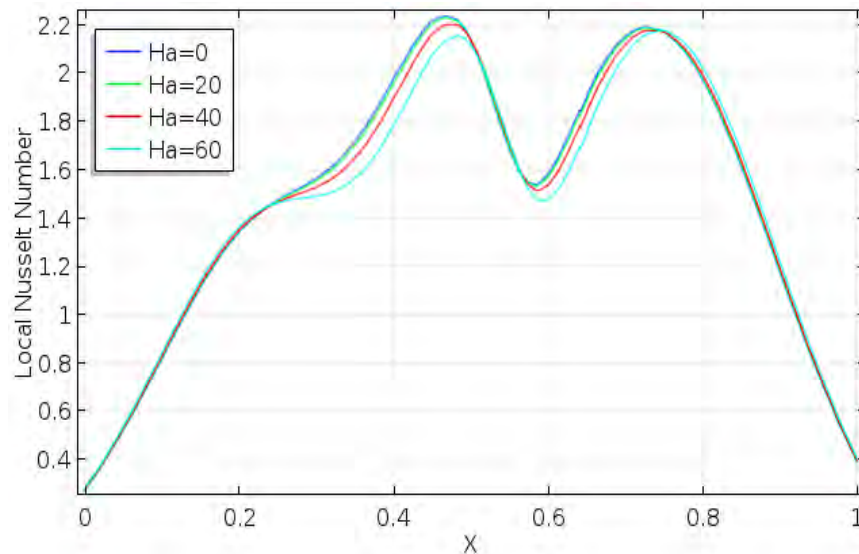


Figure 4.22: Variation of local Nusselt number along horizontal centre line of cavity for $L = 0.45$, $B = 0.04$, $D = 0.50$, $Ri = 1$ and $Pr = 0.71$ varying Ha

The variation of the local Nusselt number distribution along the horizontal centre line of the enclosure for $D = 0.50$, $Pr = 0.71$, $L = 0.45$ and $Ri = 1$ varying Hartmann number (Ha) is shown in Figure 4.22. It can be seen from the figure that the changing rate of local Nusselt number is similar for every Hartmann number but different from each other. Moreover, the local Nusselt number has two concaves up and two concaves down the effect of Hartmann number.

4.3.3 Heat Transfer Rates

In this section, results of the numerical investigation of mixed convection heat transfer in presence of magnetic field in a lid-driven wavy cavity having vertical fin are numerically presented. The average Nusselt number versus Hartmann numbers and Richardson numbers heat transfer rates are shown in Figure 4.23-4.24 and heat transfer rates Table 4.5-4.6 given below.

Table 4.5: Numerical values of average temperature of the fluid against Ri for selected value Ha while $Pr = 0.71$, $L = 0.45$, $B = 0.04$ and $D = 0.50$

Ha	Average Nusselt Number (Nu_{av})			
	$Ri = 0.1$	$Ri = 1$	$Ri = 5$	$Ri = 10$
0	6.8217	6.8786	7.2917	7.6491
20	6.7948	6.8405	7.2264	7.5774
40	6.7801	6.8277	7.2179	7.5638
60	6.7693	6.8163	7.2056	7.5490

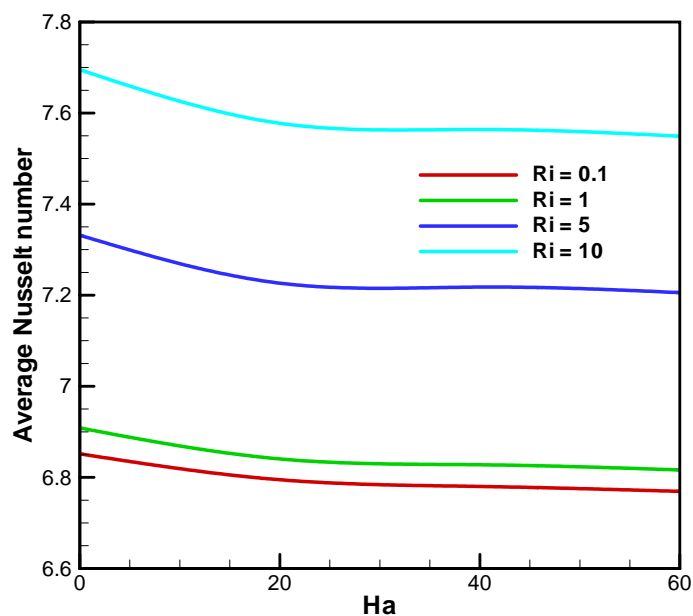


Figure 4.23: Variation of the average Nusselt number against Ha for selected value Ri while $Pr = 0.71$, $L = 0.45$, $B = 0.04$ and $D = 0.50$

Figure 4.23 depict that the average Nusselt number (Nu_{av}) versus Hartmann number along the right cold wall for various Richardson number (Ri) with fin length $L = 0.45$ while the value of the remaining parameters is kept fixed. It can be seen from this figure, the average Nusselt number increases when the value of the Richardson number increases. At a constant Richardson number, with a decrease in Hartmann number the buoyancy force increases and the heat transfer are enhanced.

Table 4.6: Numerical values of average temperature of the fluid against Ri for selected value Ha while $Pr = 0.71$, $L = 0.45$, $B = 0.04$ and $D = 0.50$

Ri	Average Temperature (θ_{av})			
	$Ha = 0$	$Ha = 20$	$Ha = 40$	$Ha = 60$
4	0.50535	0.50380	0.50300	0.50276
1	0.51077	0.50924	0.50839	0.50813
5	0.52929	0.52568	0.52345	0.52270
10	0.53403	0.52920	0.52627	0.52530

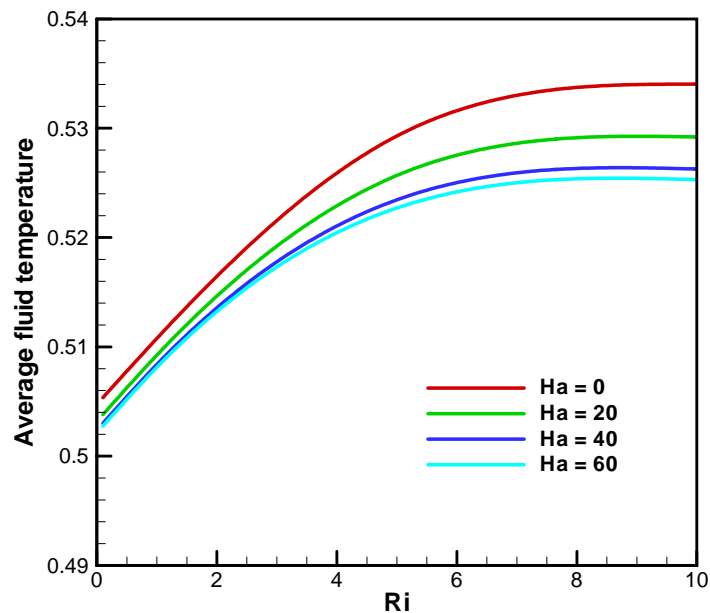


Figure 4.24: Variation of the average fluid temperature against Ri for selected value Ha while $Pr = 0.71$, $L = 0.45$, $B = 0.04$ and $D = 0.50$

Figure 4.24 illustrate the average fluid temperature (θ_{av}) versus Richardson number (Ri) for various values of Hartmann number (Ha) with the fin length $L = 0.45$, while the value of the remaining parameters is kept constant. It can be seen from this figure, average fluid temperature increases when the value of Hartmann number decreases. It is also seen from this figure, average fluid temperature increases steadily with increasing value of Richardson number when Hartmann number is kept constant.

Table 4.5 - 4.6 represent the values of the average Nusselt number and average fluid temperature respectively for considered parameters including Ri , Pr , Ha , $L = 0.45$ and B respectively. Both the numerical result indicates that the average Nusselt number and average fluid temperature increases with increasing the value of Ri and decrease with the higher value of Ha .

Finally, both heat transfer rate and average temperature increase with increasing of Richardson number for all values of Hartmann number. At a constant Hartmann number, with the increase in Richardson number the buoyancy force increases and heat transfer is enhanced.

4.4 FIN EFFECTIVENESS

In this section, results of the numerical investigation of mixed convection heat transfer in presence of magnetic field in a lid-driven wavy cavity having vertical fin are numerically presented. The results have been obtained fin effectiveness for the Richardson number versus Hartmann number. The results of this parametric study are shown in Figure 4.25- 4.28 and numerical values are shown in Table 4.7- 4.10.

Table 4.7: Numerical values of fin effectiveness as a function of Ri for different values of Ha while $Pr = 0.71$, $L = 0.25$, $B = 0.04$ and $D = 0.50$

Ri	Fin Effectiveness (ϵ_f)			
	$Ha = 0$	$Ha = 20$	$Ha = 40$	$Ha = 60$
0.1	1.081425	1.080930	1.079222	1.075849
1	1.087349	1.087252	1.086481	1.084033
5	1.103860	1.103765	1.103278	1.101785
10	1.118086	1.117703	1.116529	1.114484

The below Figure 4.25 depict that the effect of Richardson number on fin effectiveness (ϵ_f) while the controlling parameters are $Pr = 0.71$, $Ha = 0, 20, 40, 60$, $L = 0.25$, $B = 0.04$ and $D = 0.50$. It can be seen from this figure, the fin effectiveness increases associated with the increasing values of the Richardson number when the

Hartmann number is kept constant. It is also seen from this figure, fin effectiveness increases steadily due to decreasing the Hartmann number when the Richardson number is kept unchanged. In this case, the maximum and minimum fin effectiveness are 1.118086 and 1.075849 respectively which is $\epsilon_f > 1$ indicates that the fins are enhancing heat transfer from the enclosure.

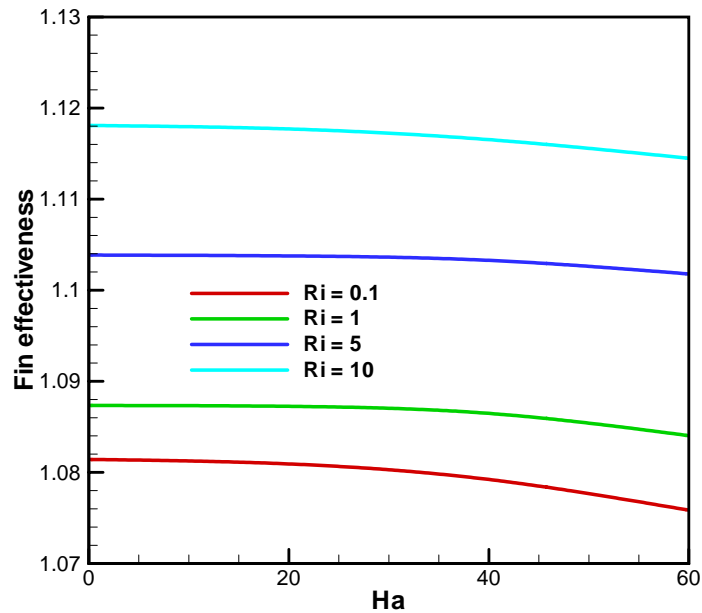


Figure 4.25: Variation of fin effectiveness against Ha for selected value of Ri while $Pr = 0.71$, $L = 0.25$, $B = 0.04$ and $D = 0.50$

Table 4.8: Numerical values of fin effectiveness as a function of Ri for different values of Ha while $Pr = 0.71$, $L = 0.35$, $B = 0.04$ and $D = 0.50$

Ri	Fin Effectiveness (ϵ_f)			
	$Ha = 0$	$Ha = 20$	$Ha = 40$	$Ha = 60$
0.1	1.132538	1.132198	1.130892	1.126286
1	1.138264	1.138125	1.138077	1.135724
5	1.153317	1.153249	1.153224	1.152160
10	1.169180	1.168798	1.167629	1.165381

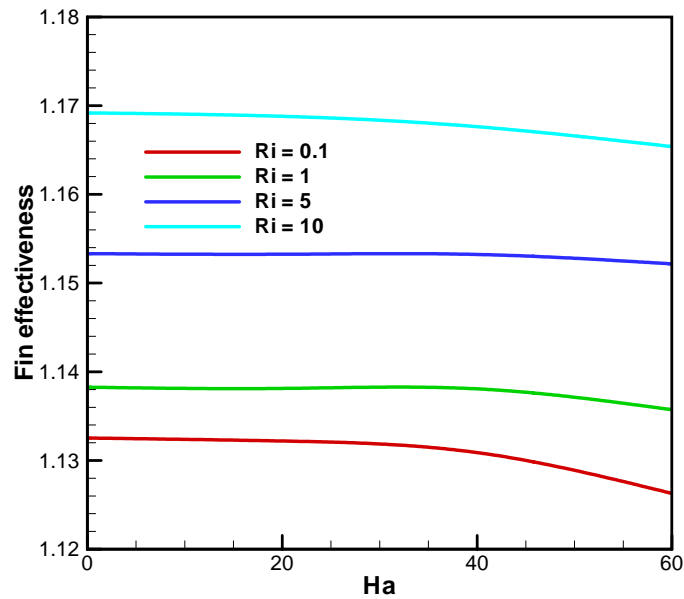


Figure 4.26: Variation of fin effectiveness against Ha for for selected value of Ri while $Pr = 0.71$, $L = 0.35$, $B = 0.04$ and $D = 0.50$

The above Figure 4.26 depict that the effect of Richardson number on fin effectiveness (ϵ_f) while the controlling parameters are $Pr = 0.71$, $Ha = 0, 20, 40, 60$, $L = 0.35$, $B = 0.04$ and $D = 0.50$. It can be seen from this figure, the fin effectiveness increases associated with the increasing Ri when the Hartmann number is kept constant. In this case, the maximum and minimum fin effectiveness are 1.169180 and 1.126286 respectively which is $\epsilon_f > 1$ indicates that the fins are enhancing heat transfer from the cavity

Table 4.9: Numerical values of fin effectiveness as a function of Ri for different values of Ha while $Pr = 0.71$, $L = 0.45$, $B = 0.04$ and $D = 0.50$

Ri	Fin Effectiveness (ϵ_f)			
	$Ha = 0$	$Ha = 20$	$Ha = 40$	$Ha = 60$
0.1	1.183970	1.183324	1.180897	1.175560
1	1.187686	1.187577	1.187263	1.184662
5	1.197163	1.197054	1.196953	1.195186
10	1.211730	1.211083	1.209867	1.207140

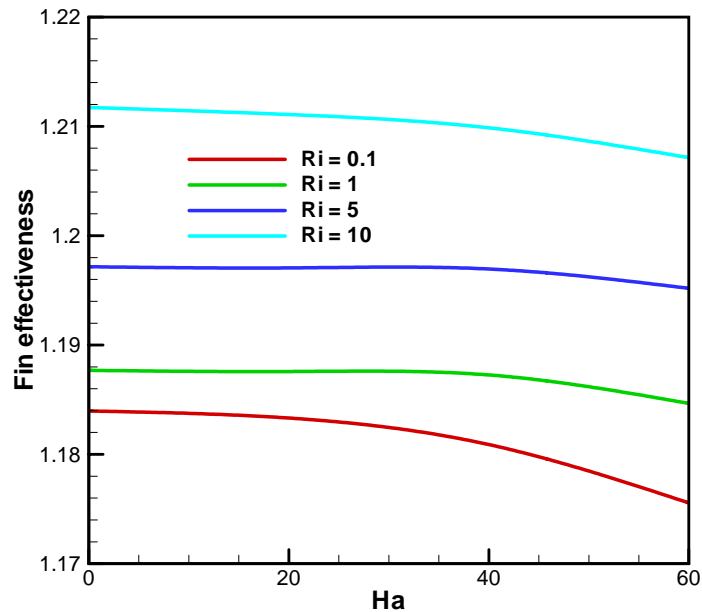


Figure 4.27: Variation of fin effectiveness against Ha for for selected value of Ri while $Pr = 0.71$, $L = 0.45$, $B = 0.04$ and $D = 0.50$

The above Figure 4.27 depict that the effect of Richardson number on fin effectiveness (ϵ_f) while the controlling parameters are $Pr = 0.71$, $Ha = 0, 20, 40, 60$, $L = 0.45$, $B = 0.04$ and $D = 0.50$. It can be seen from this figure, the fin effectiveness increases associated with the increasing values of the Richardson number when the Hartmann number is kept constant. It is also seen from this figure, fin effectiveness increases steadily due to decreasing Ha when Ri is kept unchanged. In this case, the maximum and minimum fin effectiveness are 1.211730 and 1.175560 respectively which is $\epsilon_f > 1$ indicates that the fins are enhancing heat transfer from the cavity.

Table 4.10: Numerical values of fin effectiveness as a function of fin length for different values of Ri while $Pr = 0.71$, $Ha = 20$, $B = 0.04$ and $D = 0.50$

L	Fin effectiveness (ϵ_f)			
	$Ri = 0.1$	$Ri = 1$	$Ri = 5$	$Ri = 10$
0.25	1.080930	1.087252	1.103765	1.117703
0.35	1.132198	1.138125	1.153249	1.168798
0.45	1.183324	1.187577	1.197054	1.211083

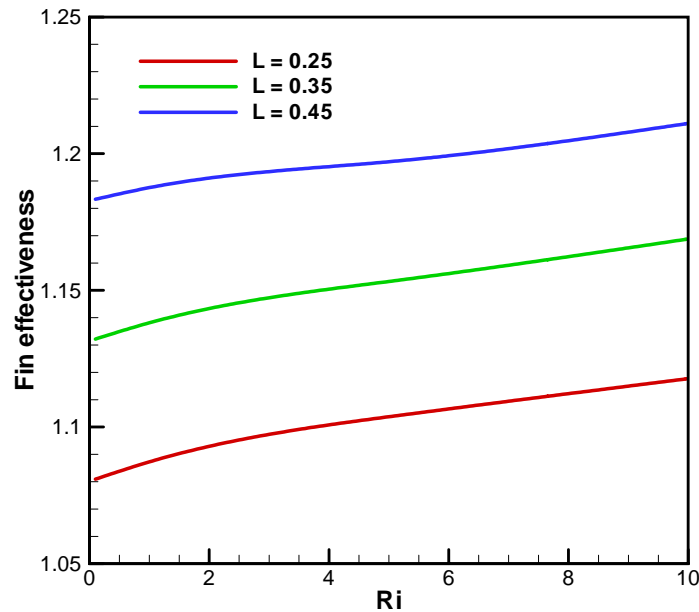


Figure 4.28: Variation of fin effectiveness against Ri for selected value of L while $Pr = 0.71$, $Ha = 20$, $B = 0.04$ and $D = 0.50$

The above Figure 4.28 depict that the effect of fin length on fin effectiveness while the controlling parameters are $Pr = 0.71$, $Ri = 0.1, 1, 5, 10$, $Ha = 20$, $B = 0.04$ and $D = 0.50$. It can be seen from this figure, the fin effectiveness increases associated with increasing values of fin length when the Richardson number is kept constant. It is also seen from this figure, fin effectiveness increases steadily due to increasing the Richardson number when the fin length is kept unchanged. In this case, the maximum fin effectiveness is 1.211083 at the fin length $L = 0.45$ and $Ri = 10$.

Table 4.7 - 4.10 represent the values of fin effectiveness for considered parameters including Ri , Pr , Ha , L , B respectively. The numerical result indicates that the fin effectiveness increases with the increased value of Ri and L and decrease with the higher value of Ha . Moreover, fin effectiveness is greater than 1 for each fin length and $\varepsilon_f > 1$ indicates that the performance of the fins is enhancing heat transfer from the enclosure.

CHAPTER 5

CONCLUSION AND RECOMMENDATIONS

The effect on the flow structure and heat transfer behaviors for mixed convection heat transfer in presence of magnetic field in a lid-driven wavy cavity having vertical fin has been studied numerically. Finite element method is used to solve governing equations. Comparisons with the published works are performed and found to be in excellent agreement. The influences of Richardson number, Hartmann number and size of fin length of the wavy cavity have been reported. The various ideas and results have been discussed in detail in the relevant chapters of the thesis. In the present chapter, an attempt is made to summarize the concepts presented and results obtained in the work reported already. A section on the scope of further work on associated fields of investigation is also included.

SUMMARY OF THE MAJOR OUTCOMES

Three different fin length as Case-1 ($L = 0.25$), Case-2 ($L = 0.35$) and Case-3 ($L = 0.45$) where Prandtl number chosen as $Pr = 0.71$ is used.

The following conclusions can be drawn from the present study:

- (i) Flow strength and heat transfer increases with increasing Richardson number in all cases. As the Richardson number increases the velocity profiles, local Nusselt number and the heat transfer rate as well as the average Nusselt number changes. The best result is found at Case-3, for the highest value of Richardson number. The mixed convection parameter Ri has significant effects on the flow and temperature fields.
- (ii) Flow structure and heat transfer reduces with increasing of Hartmann number in all cases. No significant change occurred in isotherms for all values Hartmann number. Velocity profiles, local Nusselt number, average Nusselt number and the average fluid temperature changes from highest to lowest as Ha changes lowest to highest.

- (iii) The influence of the fin length on fluid flow and temperature field is found to be pronounced in all cases. As the fin length increases the heat transfer rate as well as the average Nusselt number and average fluid temperature changes. The best result is found at $L = 0.45$.
- (iv) The maximum rate of heat transfer is obtained for the highest Ri with the lowest Ha at the fin length $L = 0.45$.
- (v) The fin effectiveness is enhanced by increasing Ri for different values of Ha . It is also found that the fin effectiveness increases with the increase of the fin length.
- (vi) The highest fin effectiveness for fin length ($L=0.45$) and Richardson number ($Ri = 10$) is found at the lowest Hartmann number ($Ha = 0$).

EXTENSION OF THIS WORK

The following can be put forward for the further works as follow-ups of the present research as.

- ❖ Double-diffusive mixed convection can be analyzed through including the governing equation of concentration conservation.
- ❖ Steady flow is considered in this thesis; it can be extended to the unsteady case.
- ❖ Only single fin is considered in this thesis, it can be extended to the parallel or series fins.
- ❖ The study can be extended for turbulent flow, different thermal boundary conditions such as constant heat flux or radiation.
- ❖ Investigation can be performed by using magnetic fluid instead of electrically conducting fluid within the porous medium.
- ❖ Two-dimensional fluid flow and heat transfer has been analyzed in this thesis. So this deliberation may be extended to three-dimensional analyses.
- ❖ The study can be extended by choosing different shapes of the cavity.
- ❖ The study can be extended for Nano-fluids.

REFERENCES

- [1] K. D. Hagen, “Heat Transfer with Applications”, 1st ed., Prentice-Hall International (1999).
- [2] Y. A. Çengel and J. M. Cimbala, “Fluid Mechanics: Fundamentals and Applications”, 3rd ed., McGraw-Hill (2014)
- [3] J. A. Shercliff, “A Textbook of Magnetohydrodynamics”, 1st ed., Pergamon Press, UK, (1965).
- [4] S. Mahmud, P. K. Das, N. Hyder and A. K. M. S. Islam, “Free convection in an enclosure with vertical wavy walls”, *Int. J. Therm. Sci.*, vol. 41, pp. 440–446 (2002).
- [5] P. K. Das and S. Mahmud, “Numerical investigation of natural convection inside a wavy enclosure”, *Int. J. Therm. Sci.*, vol. 42, pp. 397–406 (2003).
- [6] A. Misirlioglu, A.C. Baytas and I. Pop, “Natural convection inside an inclined wavy enclosure filled with a porous medium”, *Transp. Porous Media*, vol. 64, pp. 229–246 (2006).
- [7] A. Al-Amiri, K. Khanafer, J. Bull and I. Pop, “Effect of sinusoidal wavy bottom surface on mixed convection heat transfer in a lid-driven cavity”, *Int. J. Heat Mass Transf.*, vol. 50, pp. 1771–1780 (2007).
- [8] J. Rostami, “Unsteady natural convection in an enclosure with vertical wavy walls”, *Heat Mass Transf.*, vol. 44, pp. 1079–1087 (2008).
- [9] M. Mansour, M. A. El-Aziz, R. Mohamed and S. E. Ahmed, “Numerical simulation of natural convection in wavy porous cavities under the influence of thermal radiation using a thermal non-equilibrium model”, *Transp. Porous Media*, vol. 86, pp. 585–600 (2011).
- [10] K. S. Mushate, “CFD prediction of natural convection in a wavy cavity filled with porous medium”, *Global J. Res. Eng.*, vol. 11, pp. 29-45 (2011)

- [11] E. Abu-Nada and A. J. Chamkha, “Mixed convection flow of a nanofluid in a lid-driven cavity with a wavy wall”, *Int. Commun. Heat Mass Transf.*, vol. 57, pp. 36–47 (2014).
- [12] M. A. Sheremet and I. Pop, “Natural convection in a wavy porous cavity with sinusoidal temperature distributions on both side walls filled with a nanofluid: Buongiorno's mathematical model”, *J. Heat Transf.*, vol. 137, pp. 072601-8 (2015).
- [13] A. Shenoy, M. Sheremet and I. Pop, “Convective flow and heat transfer from wavy surfaces: Viscous Fluids”, *Porous Media, and nanofluids*, CRC Press, Taylor & Francis Group, Boca Raton (2016).
- [14] M. Sheremet, D. Cimpean and I. Pop, “Free convection in a partially heated wavy porous cavity filled with a nanofluid under the effects of Brownian diffusion and thermophoresis”, *Appl. Therm. Eng.*, vol. 113, pp. 413–418 (2017).
- [15] H. T. Cheong, H. T. Cheong, S. Sivasankaran, S. Sivasankaran, M. Bhuvaneshwari and M. Bhuvaneshwari, “Natural convection in a wavy porous cavity with sinusoidal heating and internal heat generation”, *Int. J. Numer. Methods Heat Fluid Flow*, vol. 27, pp. 287–309 (2017).
- [16] A. I. Alsabery, T. Tayebi, A. J. Chamkha and I. Hashim, "Effect of rotating solid cylinder on entropy generation and convective heat transfer in a wavy porous cavity heated from below", *Int. Commun. Heat Mass Transf.*, vol. 95, pp. 197-209 (2018).
- [17] M. Rahman, M. Alim and M. Sarker, “Numerical study on the conjugate effect of joule heating and magneto-hydrodynamics mixed convection in an obstructed lid-driven square cavity”, *Int. Commun. Heat Mass Transf.*, vol. 37, pp. 524-34 (2010).
- [18] L. K. Saha, K. M. S. Uddin and M. A. Taher, “Effect of internal heat generation or absorption on MHD mixed convection flow in a lid driven cavity”, *American journal of Applied Mathematics*, vol. 3, pp. 20-29 (2015).

- [19] A. F. Khudheyer, “MHD mixed convection in double lid-driven differentially heated trapezoidal cavity”, vol. 4 (2015). <https://www.ijaiem.org/Volume4Issue2/IJAIEM-2015-02-17-29.pdf>
- [20] M. M. Ali, M. A. Alim and S. S. Ahmed, “Magnetohydrodynamic mixed convection flow in a hexagonal enclosure”, *Procedia Engineering*, vol. 194, pp. 479-486 (2017).
- [21] H. F. Öztop, A. Sakhrieh, E. A. Nada and K. Al-Salem, “Mixed convection of MHD flow in nanofluid filled and partially heated wavy walled lid-driven enclosure”, *Int. Commun. Heat Mass Transf.*, vol. 86, pp. 42-51 (2017).
- [22] H. R. Ashorynejad and A. Shahriari, “MHD natural convection of hybrid nanofluid in an open wavy cavity”, *Results in Physics*, vol. 9, pp. 440-455 (2018).
- [23] R. L. Frederick, Natural convection in an inclined square enclosure with a partition attached to its cold wall, *Int. J. Heat Mass Transf.*, vol. 32, pp. 87-94 (1989).
- [24] E. Bilgen, “Natural convection in cavities with a thin fin on the hot wall”, *Int. J. Heat Mass Transf.*, vol. 48, pp. 3493-3505 (2005).
- [25] X. Shi, J. M. Khodadadi, “Laminar natural convection heat transfer in a differentially heated square cavity due to a thin fin on the hot wall”, *ASME J. Heat Transf.*, vol. 125, pp. 624-634 (2003).
- [26] R. L. Frederick, A. Valencia, “Heat transfer in a square cavity with a conducting partition on its hot wall”, *Int. Commun. Heat. Mass Transf.*, vol. 16, pp. 347-354 (1989).
- [27] A. Nag, A. Sarkar, V. M. K. Sastri, “Natural convection in a differentially heated square cavity with horizontal partition plate on the hot wall”, *Comput. Methods Appl. Mech. Eng.*, vol. 110, pp. 143-156 (1993).
- [28] E. Bilgen, “Natural convection in enclosures with partial partitions”, *Renew. Energy*, vol. 26, pp. 257-270 (2002).

- [29] X. Shi, J. M. Khodadadi, “Laminar fluid flow and heat transfer in a lid-driven cavity due to a thin fin”, *ASME J. Heat Transf.*, vol. 124, pp. 1056-1063 (2002).
- [30] R. L. Frederick, S. G. Moraga, “Three dimensional natural convection in finned cubical enclosures”, *Int. J. Heat Fluid Flow*, vol. 28, pp. 289-298 (2007).
- [31] S. H. Tasnim, M. R. Collins, “Numerical analysis of heat transfer in a square cavity with a baffle on the hot wall”, *Int. Commun. Heat. Mass Transf.*, vol. 31, pp. 639-650 (2004).
- [32] H. Öztop, E. Bilgen, “Natural convection in differentially heated and partially divided square cavities with internal heat generation”, *Int. J. Heat Fluid Flow*, vol. 27, pp. 466-475 (2006).
- [33] A. Ben-Nakhi, A. J. Chamkha, “Effect of length and inclination of a thin fin on natural convection in a square enclosure”, *Numer. Heat. Transf. Part A*, vol. 50, pp. 389-407 (2006).
- [34] A. Ben-Nakhi, A. J. Chamkha, “Conjugate natural convection in a square enclosure with inclined thin fin of arbitrary length”, *Int. J. Therm. Sci.*, vol. 46, pp. 467-478 (2007).
- [35] C. Sun, B. Yu, H. F. Öztop, Y. Wang, J. Wei, “Control of mixed convection in lid-driven enclosures using conductive triangular fins”, *Int. J. Heat Mass Transf.*, vol. 54, pp. 894–909 (2011).
- [36] A. A. R. Darzi, M. Farhadi, K. Sedighi, “Numerical study of the fin effect on mixed convection heat transfer in a lid-driven cavity”, *J. Mechanical Eng. Sci.*, vol. 225, pp. 397–406 (2011).
- [37] F. Xu, J. C. Patterson, C. Lei, “Effect of the fin length on natural convection flow transition in a cavity”, *Int. J. Therm. Sci.*, vol. 70, pp. 92–101 (2013).
- [38] F. Xu, S. C. Saha, “Transition to an unsteady flow induced by a fin on the sidewall of a differentially heated air-filled square cavity and heat transfer”, *Int. J. Heat Mass Transf.*, vol. 71, pp. 236–244 (2014).

- [39] A. Elatar, M. A. Teamah, M. A. Hassab, “Numerical study of laminar natural convection inside square enclosure with single horizontal fin”, *International Journal of Thermal Sciences*, vol. 99, pp. 41-51 (2016).
- [40] F. A. Gdhaidh, K. Hussain, H. S. Qi, “Enhancement of natural convection heat transfer within closed enclosure using parallel fins”, *Int. J. Mechanical and Mechatronics Eng.*, vol. 9, pp. 457-462 (2015).
- [41] J. H. Ferziger and M. Perić, “Computational Methods for Fluid Dynamics”, 3rd ed. Springer (2002).
- [42] S. V. Patankar, “Numerical Heat Transfer and Fluid Flows” 1st ed. Hemisphere Publishing Corporation, United States of America (1980).
- [43] C. Taylor, P. Hood, “A numerical solution of the Navier–Stokes equations using finite element technique”, *Computers and Fluids*, vol. 1, pp. 73–89 (1973).
- [44] P. Dechaumphai, *Finite Element Method in Engineering*, 2nd edition, Chulalongkorn University Press, Bangkok, 1999.